Cell Reports

Article

Flotillin-Dependent Membrane Microdomains Are Required for Functional Phagolysosomes against Fungal Infections

Graphical Abstract

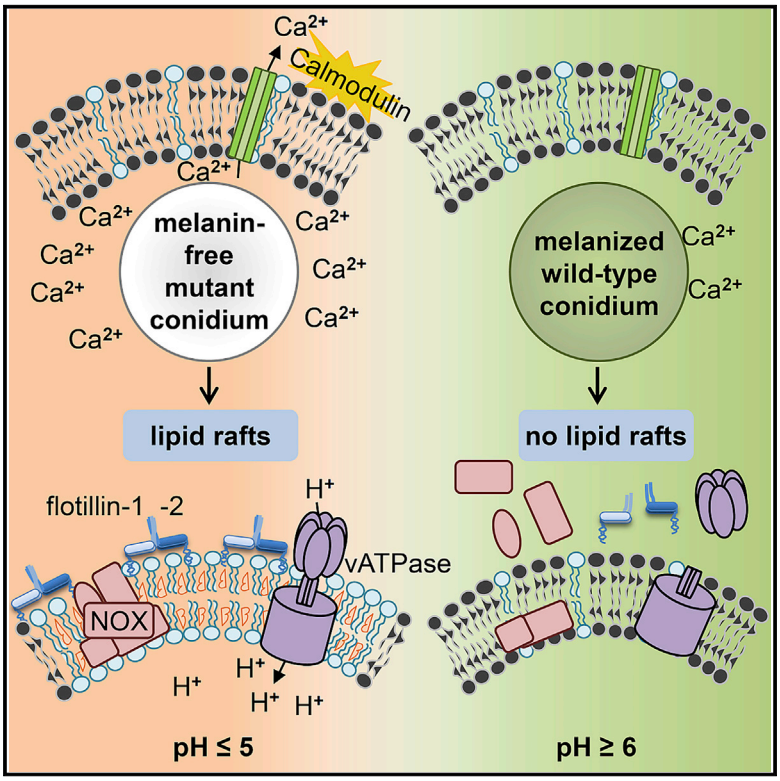

Highlights

- Lipid rafts in phagolysosomal membranes of macrophages depend on flotillins
- Both major defense complexes vATPase and NADPH oxidase require membrane microdomains
- The human-pathogenic fungus *Aspergillus fumigatus* dysregulates membrane microdomains
- An SNP in the human FLOT1 gene increases susceptibility for invasive aspergillosis

Authors

Franziska Schmidt, Andreas Thywißen, Marie Goldmann, ..., Scott G. Filler, Agostinho Carvalho, Axel A. Brakhage

Correspondence

axel.brakhage@leibniz-hki.de

In Brief

Schmidt el al. show that lipid rafts in phagolysosomal membranes of macrophages depend on flotillins. Lipid rafts are required for assembly of vATPase and NADPH oxidase. Conidia of the human-pathogenic fungus *Aspergillus fumigatus* dysregulate assembly of flotillin-dependent lipid rafts in the phagolysosomal membrane and can thereby escape phagolysosomal digestion.

Schmidt et al., 2020, Cell Reports *32*, 108017
August 18, 2020
https://doi.org/10.1016/j.celrep.2020.108017

CellPress

Cell Reports

CellPress
OPEN ACCESS

Article

Flotillin-Dependent Membrane Microdomains Are Required for Functional Phagolysosomes against Fungal Infections

Franziska Schmidt,[1,2,14] Andreas Thywißen,[1,2,14] Marie Goldmann,[1,2] Cristina Cunha,[3,4] Zoltán Cseresnyés,[5] Hella Schmidt,[1,2] Muhammad Rafiq,[1,2] Silvia Galiani,[6] Markus H. Gräler,[7] Georgios Chamilos,[8] João F. Lacerda,[9] António Campos, Jr.,[10] Christian Eggeling,[6,11] Marc Thilo Figge,[5] Thorsten Heinekamp,[1] Scott G. Filler,[12,13] Agostinho Carvalho,[3,4] and Axel A. Brakhage[1,2,15,*]

[1]Department of Molecular and Applied Microbiology, Leibniz Institute for Natural Product Research and Infection Biology – Hans Knöll Institute (HKI), 07745 Jena, Germany
[2]Department of Microbiology and Molecular Biology, Institute of Microbiology, Friedrich Schiller University Jena, 07745 Jena, Germany
[3]Life and Health Sciences Research Institute (ICVS), School of Medicine, University of Minho, Campus de Gualtar, 4710-057 Braga, Portugal
[4]ICVS/3B's - PT Government Associate Laboratory, Braga/Guimarães, Campus de Gualtar, 4710-057 Braga, Portugal
[5]Research Group Applied Systems Biology, Leibniz Institute for Natural Product Research and Infection Biology (HKI), 07745 Jena, Germany
[6]MRC Human Immunology Unit, Weatherall Institute of Molecular Medicine, University of Oxford, Headley Way, Oxford OX3 9DS, UK
[7]Department of Anesthesiology and Intensive Care Medicine, Center for Sepsis Control and Care (CSCC) and Center for Molecular Biomedicine (CMB), University Hospital Jena, 07740 Jena, Germany
[8]Department of Medicine, University of Crete, and Institute of Molecular Biology and Biotechnology, Foundation for Research and Technology, 71300 Heraklion, Crete, Greece
[9]Serviço de Hematologia e Transplantação de Medula, Hospital de Santa Maria, 1649-035 Lisboa, Portugal, and Instituto de Medicina Molecular, Faculdade de Medicina de Lisboa, 1649-028 Lisboa, Portugal
[10]Serviço de Transplantação de Medula Óssea (STMO), Instituto Português de Oncologia do Porto, 4200-072 Porto, Portugal
[11]Institute of Applied Optics, Friedrich Schiller University Jena, and Department of Biophysical Imaging, Leibniz Institute of Photonic Technology (IPHT), 07745 Jena, Germany
[12]Division of Infectious Diseases, Los Angeles Biomedical Research Institute at Harbor-UCLA Medical Center, Torrance CA 90502, USA
[13]David Geffen School of Medicine at University of California, Los Angeles, Los Angeles, CA, USA
[14]These authors contributed equally
[15]Lead Contact
*Correspondence: axel.brakhage@leibniz-hki.de
https://doi.org/10.1016/j.celrep.2020.108017

SUMMARY

Lipid rafts form signaling platforms on biological membranes with incompletely characterized role in immune response to infection. Here we report that lipid-raft microdomains are essential components of phagolysosomal membranes of macrophages and depend on flotillins. Genetic deletion of flotillins demonstrates that the assembly of both major defense complexes vATPase and NADPH oxidase requires membrane microdomains. Furthermore, we describe a virulence mechanism leading to dysregulation of membrane microdomains by melanized wild-type conidia of the important human-pathogenic fungus *Aspergillus fumigatus* resulting in reduced phagolysosomal acidification. We show that phagolysosomes with ingested melanized conidia contain a reduced amount of free Ca^{2+} ions and that inhibition of Ca^{2+}-dependent calmodulin activity led to reduced lipid-raft formation. We identify a single-nucleotide polymorphism in the human *FLOT1* gene resulting in heightened susceptibility for invasive aspergillosis in hematopoietic stem cell transplant recipients. Collectively, flotillin-dependent microdomains on the phagolysosomal membrane play an essential role in protective antifungal immunity.

INTRODUCTION

Many bacteria manipulate phagocytes to counteract immune responses. For example, *Mycobacterium* species (spp.), *Legionella* spp., and *Listeria* spp. withstand intracellular degradation after ingestion by phagocytes (Cambier et al., 2014; Carvalho et al., 2014; Ensminger, 2016). This is accomplished by their ability to interfere with the formation of a functional hostile phagolysosome.

Pathogenic fungi have also developed mechanisms to avoid being killed after they are taken up by phagocytes. The encapsulated yeast *Cryptococcus neoformans* damages phagosomal membranes, deploys antioxidant mechanisms, and manipulates phagosomal maturation, which enables the fungus to survive and replicate inside phagosomes (Levitz et al., 1999; Smith et al., 2015; Tucker and Casadevall, 2002; Zaragoza et al., 2008). Other fungi, such as the yeast forms of *Candida* spp. and *Histoplasma*

capsulatum, employ mechanisms to establish an intracellular life cycle or avoid killing inside the phagolysosome, respectively (Fernández-Arenas et al., 2009; Newman et al., 2006; Seider et al., 2011). For example, *H. capsulatum* yeast cells reduce phagosomal acidification by releasing the saposin-like protein CBP that reduces vacuolar ATPase (vATPase) accumulation on the phagosomal membrane (Batanghari et al., 1998). *Rhizopus* spp. establish intracellular persistence inside alveolar macrophages. Lack of intracellular swelling of *Rhizopus* conidia results in surface retention of melanin, which induces phagosome maturation arrest through inhibition of LC3-associated phagocytosis (LAP) (Andrianaki et al., 2018).

In line, we previously reported that the gray-greenish pigment dihydroxynaphthalene (DHN) melanin of conidia (spores) is an important virulence factor of the pathogenic fungus *Aspergillus fumigatus* that is predicted to cause more than 200,000 life-threatening infections worldwide (Brown et al., 2012; Kosmidis and Denning, 2015). DHN-melanin is responsible for establishing a non-hostile intracellular niche inside phagocytes by inhibiting phagolysosomal acidification, LAP, and apoptosis of phagocytes and as a consequence prevents killing of conidia (Akoumianaki et al., 2016; Heinekamp et al., 2013; Schmidt et al., 2018; Thywißen et al., 2011; Volling et al., 2011). DHN-melanin (Langfelder et al., 2003) plays a pivotal role in this process, because even melanin ghosts (i.e., isolated pigment particles) led to reduced acidification to the same extent as wild-type conidia and impaired LAP, whereas conidia from the pigmentless *pksP* mutant showed full acidification of phagolysosomes and full activation of LAP (Akoumianaki et al., 2016; Thywißen et al., 2011).

The effect of reduced acidification due to melanized conidia was observed in mouse and human cell lines as well as human primary cells (Jahn et al., 2002; Mohebbi et al., 2016; Overton et al., 2018; Thywißen et al., 2011). Furthermore, the absence of melanin in the *pksP* mutant results in a higher phagocytosis rate, faster endocytic processing, and increased production of pro-inflammatory cytokines and chemokines by phagocytes most likely due to better recognition of *pksP* conidia by the dectin-1 receptor (Chai et al., 2010; Luther et al., 2007; Mech et al., 2011; Thywißen et al., 2011). Further data indicated that DHN-melanin is able to abrogate the release of free Ca^{2+} ions to the peri-phagosomal area, thereby inhibiting calmodulin activity and impairing phagosome function (Kyrmizi et al., 2018).

For fungal pathogens, the molecular mechanisms involved in the dysregulation of phagolysosomes and, furthermore, many aspects of phagosome maturation are unsolved. Here, we add novel insights into both aspects by the finding of membrane microdomains contributing to phagosome maturation and defense against invasive aspergillosis (IA) and also as a target of pathogens. We discovered an unprecedented virulence mechanism depending on the inhibition of flotillin-dependent microdomain formation in phagolysosomal membranes by conidial melanin.

RESULTS

Reduced Phagolysosomal Acidification Increases Conidia-Induced Damage of Macrophages

If a macrophage ingests an *A. fumigatus* conidium and fails to kill it, the conidium swells and germinates to produce a hypha that then pierces the macrophage and eventually kills it. We used the vATPase inhibitor bafilomycin A1 to determine whether inhibition of phagolysosomal acidification affects the extent of macrophage damage. Wild-type conidia caused considerable macrophage damage, whereas *pksP*-mutant conidia lacking DHN-melanin caused significantly lower host cell damage (Figure 1A). Abolishing phagolysosomal acidification with bafilomycin A1 increased the macrophage damage caused by both wild-type and *pksP* conidia. In the presence of bafilomycin A1, wild-type and *pksP* conidia caused virtually identical host cell damage. These results indicate that the capacity of melanized conidia to reside in a phagolysosome with reduced acidification enhances the capacity of the organism to survive within the phagocyte and eventually kill it.

Reduced Acidification Is Observed in Intact Phagolysosomes Containing Melanized Conidia and Correlates with Reduced Assembly of Functional vATPase at the Phagolysosomal Membrane

Previously, we reported that wild-type conidia inhibit the acidification of phagolysosomes by using acridine orange (Jahn et al., 2002), hyperspectral imaging (Mohebbi et al., 2016), and LysoTracker red (Thywißen et al., 2011). Here, we further confirmed this data by applying pHRodo to RAW 264.7 macrophages (Figures S1A and S1B) that showed ~10% of wild-type conidia in acidified phagolysosomes in contrast to *pksP* conidia, of which >90% were found in acidified phagolysosomes. To investigate whether the inhibition of acidification by wild-type conidia is a global phenomenon or is limited to phagolysosomes that contain melanized conidia, macrophages were loaded with LysoTracker red and simultaneously infected with melanized wild-type and pigmentless *pksP* conidia. We found single macrophages infected with both conidia simultaneously (i.e., wild-type and *pksP* conidia). In such macrophages, there was no acidification of phagolysosomes containing wild-type conidia but clear acidification of phagolysosomes containing *pksP* conidia (Figures 1B and 1C).

In theory, the reduction of acidification by wild-type conidia could be due to a disruption of the lysosomal membrane. To exclude this possibility, we measured protein CHMP4B as part of the endosomal sorting complexes required for transport (ESCRT)-III complex that is recruited to damaged endosomes (Skowyra et al., 2018). We did not observe any recruitment of CHMP4B to phagolysosomes after 2 h of coincubation, the time point at which we measured acidification (Figure S1D). This finding was confirmed by measuring galectins that represent cytosolic damage sensors due to their binding to luminal glycans exposed on leaky organelles such as phagolysosomes (Skowyra et al., 2018). Using an anti-galectin antibody, there were no galectin-specific signals surrounding phagolysosomes that contained wild-type or *pksP* conidia (Figure S1E). Damage induced by L-leucyl-L-leucine methyl ester (LLOMe) was used as positive control (Maejima et al., 2013; Thiele and Lipsky, 1990). These data exclude that at the time point of our measurements significant damage of phagolysosomes had occurred. This is also supported by our notion that isolated phagolysosomes containing conidia could be isolated and stained (Figure 5).

Based on the observation of reduced acidification, we hypothesized that wild-type conidia-containing phagolysosomal

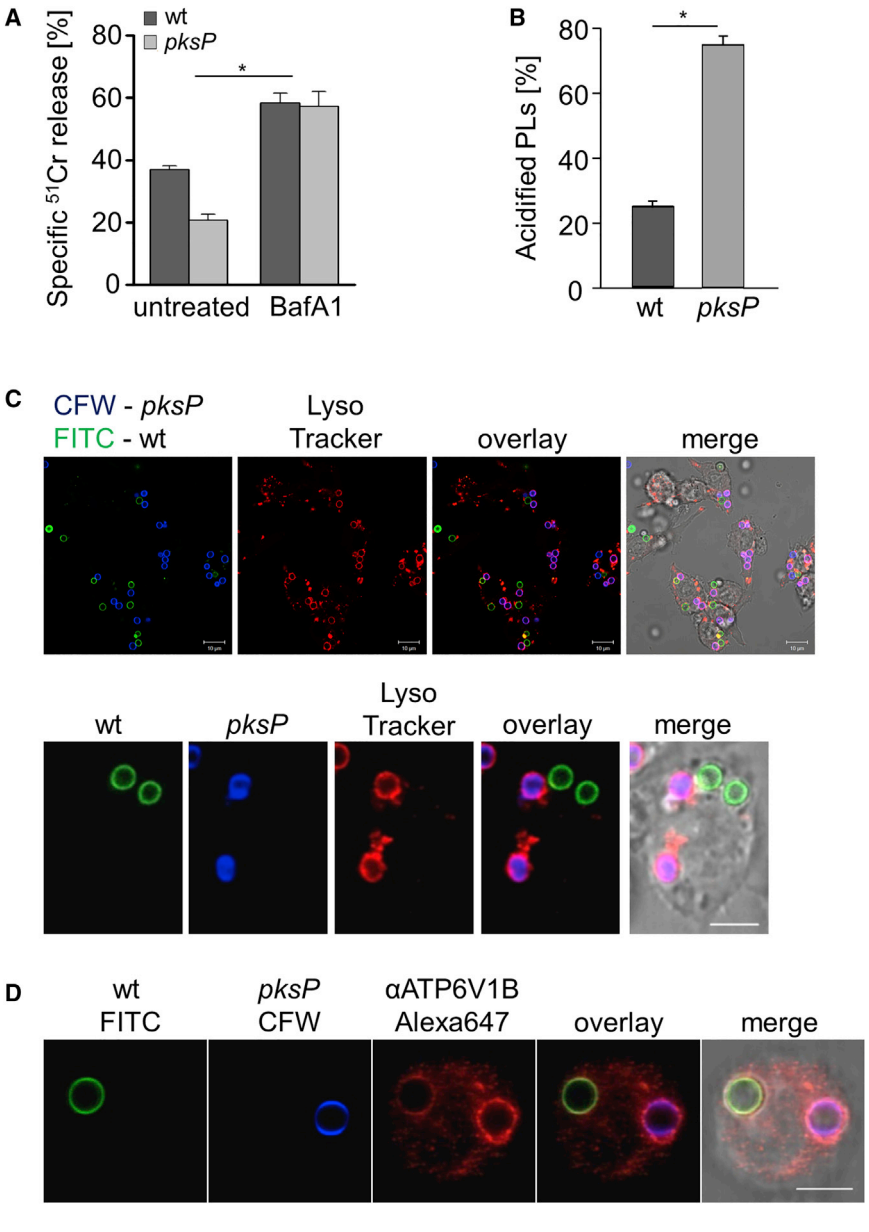

Figure 1. *A. fumigatus* Melanized Wild-Type Conidia Increase Host Cell Damage and Reduce Functionality of Phagolysosomes

(A) Cell damage monitored by ^{51}Cr release from RAW264.7 macrophages infected with *A. fumigatus* wild-type or *pksP* conidia. Data represent mean ± SD; $p < 0.05$.

(B) Acidified phagolysosomes (PLs) were stained with LysoTracker red. RAW264.7 macrophage cells were infected with wild-type and *pksP* conidia for 2 h at MOI = 2. Data represent mean ± SD; $p < 0.001$.

(C) RAW264.7 cells had simultaneously phagocytosed melanized wild-type conidia (labeled with fluorescein isothiocyanate [FITC], green) and non-pigmented *pksP* conidia (labeled with Calcofluor white [CFW], blue). Acidified phagolysosomes were stained with LysoTracker red. Scale bar, 10 μm. Lower panel shows a single cell. Scale bar, 5 μm.

(D) A RAW264.7 macrophage had simultaneously phagocytosed a wild-type conidium (FITC labeled) and a *pksP* conidium (CFW labeled). Localization of cytoplasmic vATPase subunit V_1 to the phagolysosomal membrane was monitored by immunofluorescence. Scale bar, 5 μm.

See also Figure S1.

membranes contain less active vATPase that consists of two complexes. The V_0 complex is integrated into the membrane and, when assembled with the cytoplasmic V_1 complex, shuttles protons across the lipid bilayer (Cotter et al., 2015). To analyze the binding of V_1 to the V_0 complex, localization of the V_1 complex to the membranes of phagolysosomes that contained either wild-type or *pksP* conidia was monitored by immunofluorescence. In the same macrophage, we only found faint staining of the phagolysosomal membrane that surrounded wild-type conidia (Figure 1D). By contrast, there was a strong signal for V_1 at the membrane surrounding *pksP* conidia. Quantification of vATPase assembly revealed that <30% of phagolysosomes containing a wild-type conidium showed recruitment of V_1 to the membrane compared to nearly 70% of phagolysosomes with an ingested *pksP* conidium (Figure S1C). This finding agrees with our previous data obtained by proteome analysis of phagolysosomes, where an increased abundance of V_1 in phagolysosomes containing *pksP* conidia was detected compared with phagolysosomes containing wild-type conidia (Schmidt et al., 2018).

Melanized Conidia Interfere with the Formation of Membrane Microdomains in Phagolysosomes

The reduced vATPase in the phagolysosomal membrane implied that the formation of membrane microdomains, also known as lipid rafts (Lingwood and Simons, 2010), was disturbed in phagolysosomes with DHN-melanin-containing conidia. Therefore, the presence of several lipid-raft marker lipids such as cholesterol and sphingolipids was analyzed. For this purpose, macrophages were infected with melanized and *pksP* conidia and then stained with fluorescently labeled cholera toxin subunit B (CTB) to label the sphingolipid GM1 ganglioside, whose accumulation at distinct membrane sites is characteristic of lipid rafts. In MH-S and RAW264.7 murine macrophages as well as in primary human macrophages that had ingested melanized conidia, there was only minimal CTB staining of the phagolysosomal membrane, despite CTB staining of the macrophage cytoplasmic membrane (Figures 2A, 2B, and S2A–S2C). By contrast, in macrophages that had ingested *pksP* conidia, distinct CTB staining of both the phagolysosomal and cytoplasmic membranes was

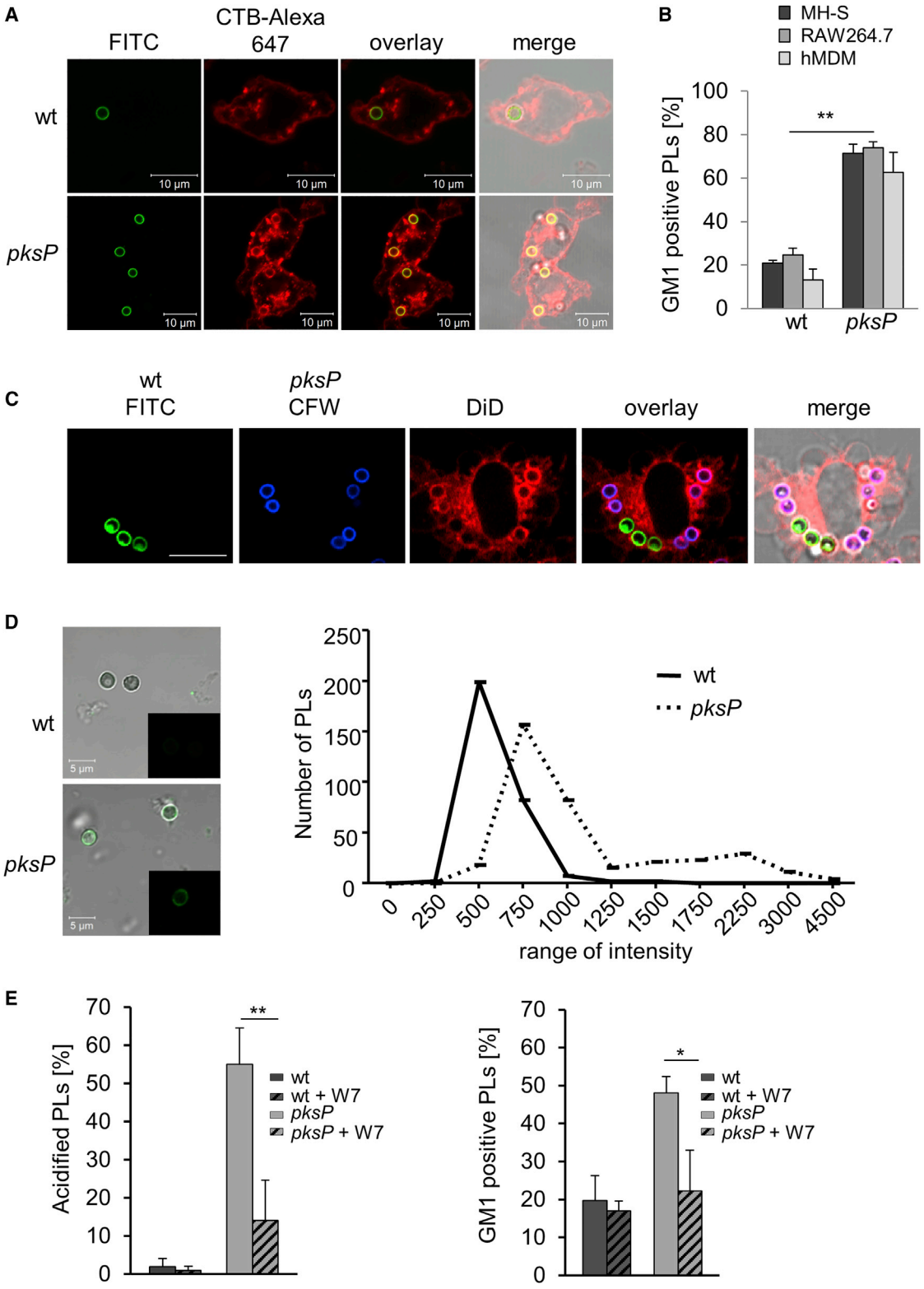

Figure 2. *A. fumigatus* Conidia Interfere with Phagolysosomal Lipid-Raft Formation

(A) RAW264.7 macrophages stained for GM1 ganglioside (CTB-Alexa Fluor 647, red) were infected with FITC-labeled wild-type or *pksP* conidia.

(B) Quantification of GM1-positive phagolysosomes (PLs) in murine MH-S and RAW264.7 macrophages as well as human monocyte-derived macrophages (hMDM) after infection with wild-type or *pksP* conidia. Data are presented as mean ± SD; $p < 0.05$.

(legend continued on next page)

visible. Further analysis confirmed that there was no difference in GM1 staining in the cytoplasmic membrane irrespective of whether cells had ingested wild-type or *pksP* conidia (Figures S2A–S2C).

To further substantiate this finding, the lipophilic dye DiD was used. As shown by confocal laser scanning microscopy, DiD only weakly labeled membranes surrounding melanized conidia but strongly labeled membranes enclosing *pksP* conidia (Figure 2C). The percentage of DiD-positive phagolysosomes containing wild-type conidia was significantly reduced compared to phagolysosomes with *pksP* conidia (Figure S2D). These results confirmed that the presence of DHN-melanin on the ingested conidium affects the lipid composition of the phagolysosomal membrane.

To determine the relationship between membrane microdomains and phagolysosomal acidification, we demonstrated that phagolysosomes containing melanized conidia were neither acidified nor contained GM1-stained membrane microdomains, whereas phagolysosomes containing *pksP* conidia contained acidified endosomal and lysosomal vesicles that strongly colocalized with microdomains (Figures S3A–S3D), as also visualized by 3D reconstruction (Videos S1 and S2). In additional experiments, we demonstrated that the observed effects were due to DHN-melanin, because melanin ghosts had the same capacity as wild-type conidia to reside in nonacidified phagolysosomes with reduced formation of microdomains (Figure S3E). Collectively, these data indicate that lipid-raft formation correlates with the acidification of the phagolysosome and that these processes are reduced in phagolysosomes containing melanized conidia.

To determine whether reduced microdomain formation influences phagolysosome acidification, macrophages were treated with methyl-β-cyclodextrin (MβCD), which depletes the cells of cholesterol and consequently disrupts the membrane. MβCD treatment reduced the total cellular cholesterol content to <20% compared to the untreated control (Figure S4). Exposure to MβCD resulted in a complete absence of acidification of the phagolysosome as well as almost all of the endosomal and lysosomal vesicles. Although ~10% of phagolysosomes containing melanized or *pksP* conidia still stained positive for GM1, acidification of these phagolysosomes was almost completely abolished. Thus, the presence of microdomains in the phagolysosomal membrane contributes to proper acidification.

Inhibition of Calmodulin Activity Reduces Formation of Microdomains in the Phagolysosomal Membrane

Previously we showed that melanized conidia reduce the release of free Ca^{2+} ions from the phagosome lumen to the peri-phagosomal area, thereby preventing activation of calmodulin and LAP (Kyrmizi et al., 2018). Thus, it was conceivable that a change of the endosomal Ca^{2+} concentration by DHN-melanin also dysregulates membrane microdomain formation. We first tested the presence of Ca^{2+} ions in phagolysosomes containing melanized and *pksP* conidia using Fluo-4. For *pksP* conidia, a much higher content of free Ca^{2+} ions was detected compared to wild-type conidia-containing phagolysosomes (Figure 2D). Because calmodulin is a central Ca^{2+}-sensing regulatory kinase (Villalobo, 2018), we inhibited calmodulin activity by addition of the inhibitor W7. This led to reduced formation of membrane microdomains and reduced acidification of *pksP*-containing phagolysosomes (Figure 2E). Our data thus suggest that the activation of calmodulin contributes to lipid-raft formation and its inhibition by the capability of DHN-melanin to change the endosomal Ca^{2+} concentration reduces formation of lipid rafts.

Membrane Microdomains of RAW264.7 Macrophages Contain Flotillin, but Not Caveolin

The role of lipid-raft microdomains for phagosome biogenesis and their composition in the phagosomal membrane are unknown. Nevertheless, the differentiation of membrane microdomains into sub-classes of lipid-raft domains and caveolae domains is widely accepted (Lingwood and Simons, 2010; Pike, 2009). Whereas both caveolin-1 and caveolin-2 were detected in control HeLa cells by immunofluorescence or immunoblotting, in RAW264.7 macrophages these proteins were absent (Figure 3A), as previously also shown by western blot for caveolin-1 and caveolin-2 (Martínez-Mármol et al., 2008; Matveev et al., 1999). By contrast, flotillin-1 (Flot-1), a marker for a different subset of lipid rafts and assumed to act as scaffolding protein that stabilizes membrane microdomains (Otto and Nichols, 2011; Stuermer, 2011), colocalized with GM1 ganglioside on phagolysosomal membranes of RAW264.7 cells containing *pksP* conidia but not melanized conidia (Figures 3B, 3C, and S9A). These data indicate that *pksP* but not wild-type conidia reside in phagolysosomes containing flotillin-dependent microdomains in their membrane.

The Number of *pksP* Conidia Residing in Acidified Phagolysosomes Is Drastically Reduced in Macrophages of *Flot-1*/*Flot-2* Double-Knockout Mice

In mice and humans, two flotillins are known, Flot-1 and flotillin-2 (Flot-2) (Frick et al., 2007). Both isoforms are integrated in membrane microdomains by N-terminal hairpin structures and together with other proteins they form hetero-oligomeric complexes (Solis et al., 2007). Since Flot-1 was identified in the membrane of *pksP*-containing phagolysosomes (Figure S5A), we analyzed the effects of flotillins on phagolysosome function. Knockdown of either *Flot-1* or *Flot-2* in the murine macrophage-like cell line J774A.1 (Figure S5B) reduced the acidification of phagolysosomes containing *pksP* conidia; the effect

(C) DiD stains lipids in membranes. Wild-type conidia and *pksP* conidia were stained with FITC (green) and CFW (blue), respectively. RAW264.7 cells were treated with DiD and infected for 2 h with *pksP* and wild-type conidia at MOI = 2. Scale bar, 10 μm.
(D) Ca^{2+} ions in purified phagolysosomes (PLs) of RAW264.7 cells containing wild-type and *pksP* conidia stained with Fluo-4 (microscopic images) and their quantification. The average fluorescence intensity was calculated using ImageJ software for three biological replicates. Total number of counted phagolysosomes: n = 360 for *pksP*, n = 290 for wild-type conidia. Statistical analysis was performed using two-tailed unequal variance Student's t test. p = 0.0005.
(E) Acidification of phagolysosomes (PLs) and GM1 staining of phagolysosomes containing the indicated conidia upon addition of the calmodulin inhibitor W7.
See also Figures S2–S4.

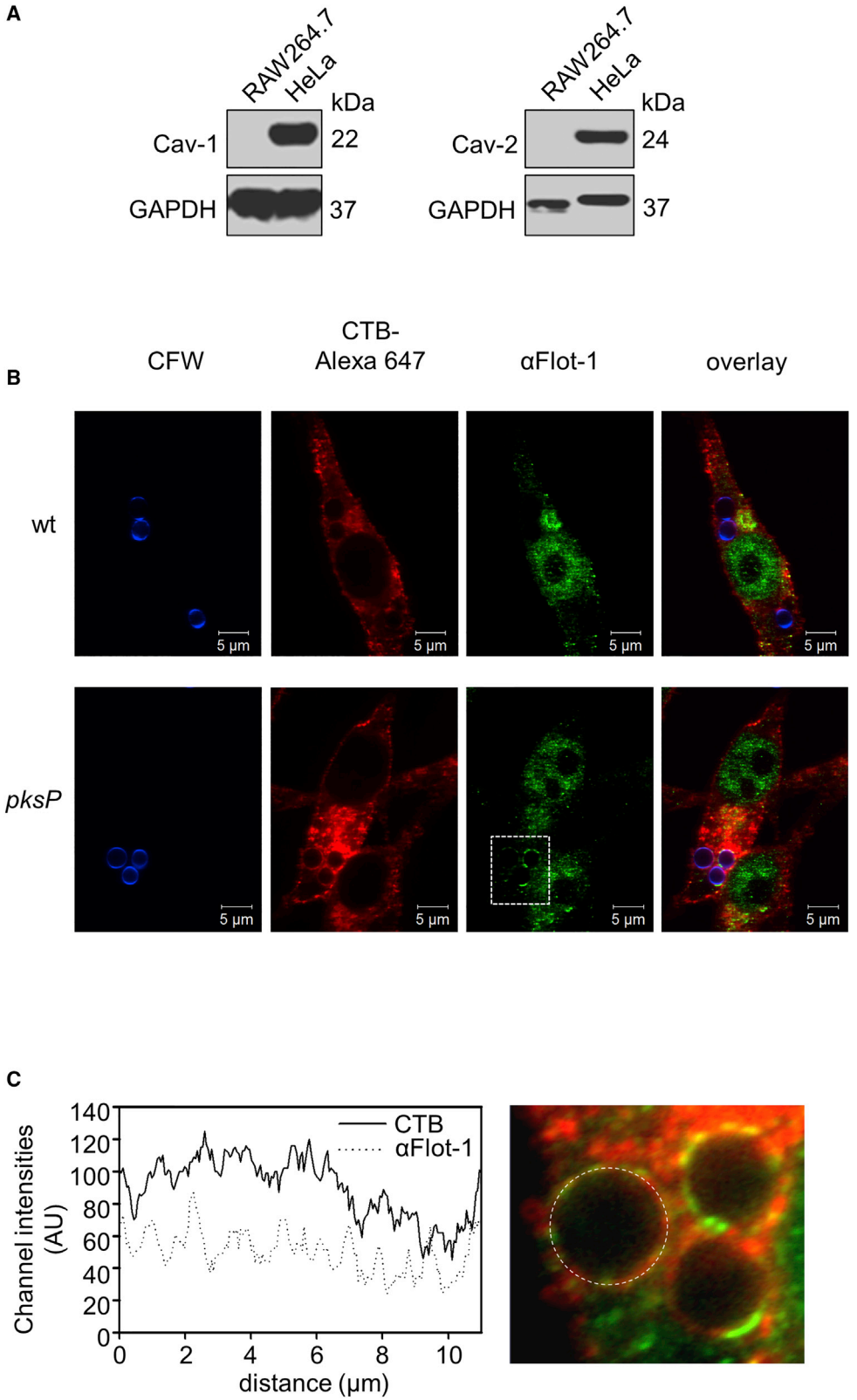

(legend on next page)

due to knockdown of *Flot-1* was more pronounced (Figure S5C). Simultaneous knockdown of both *Flot-1* and *Flot-2* further decreased the percentage of acidified phagolysosomes containing wild-type conidia. This initial finding was substantiated and evaluated by the analysis of bone-marrow-derived macrophages (BMDMs) from *Flot-1/Flot-2* double-knockout ($Flot^{-/-}$) mice (Bitsikas et al., 2014). Compared to C57BL/6 wild-type mice, BMDMs of $Flot^{-/-}$ mice showed impaired acidification of phagolysosomes containing *pksP* conidia (Figure 4A). As expected, wild-type conidia containing phagolysosomes showed no significant acidification. Absence of flotillins did not fully inhibit acidification but resulted in a significant delay of phagolysosomal acidification (Figure S5D).

We also confirmed that in mouse BMDMs, acidification of conidia-containing phagolysosomes was dependent on membrane microdomains. In primary macrophages, only ~5% of phagolysosomes containing wild-type conidia were acidified, and this percentage was further reduced by treatment with MβCD. Furthermore, no phagolysosomal acidification was detectable in $Flot^{-/-}$ macrophages treated with MβCD (Figure 4A). The number of acidified phagolysosomes containing *pksP* conidia was drastically reduced by treatment with MβCD and was not further decreased in $Flot^{-/-}$ macrophages treated with MβCD, indicating that flotillin and cholesterol function in the same pathway to enable phagolysosomal acidification. These results were further underlined by using *Flot-1/Flot-2* double-knockout BMDMs which clearly showed reduced amount of lipid-raft microdomains indicated by GM1 staining in the membrane of phagolysosomes containing either wild-type or *pksP* conidia (Figures 4B and 4C).

Assembly of vATPase and NADPH Oxidase and Phagocytosis of Conidia Depend on Flotillin-Containing Membrane Microdomains

Previous studies reported that in maturing phagosomes, vATPase is assembled in membrane microdomains (Dermine et al., 2001; Lafourcade et al., 2008). To provide evidence that flotillin as a lipid-raft chaperone is in fact required for this process, the assembly of vATPase in macrophages isolated from wild-type and $Flot^{-/-}$ mice, was quantified (Figure 5A). The percentage of phagolysosomal membranes showing a high degree of assembled vATPases when *pksP* conidia were ingested was reduced from 30% in wild-type macrophages to about 10 % in $Flot^{-/-}$ macrophages, indicating the dependency of vATPase assembly on flotillins, as earlier shown for cells of the murine macrophage-like cell line J774A.1 (Dermine et al., 2001). Stimulated emission depletion (STED) microscopy confirmed colocalization of Flot-1 with the vATPase V_1 complex at the phagolysosomal membrane (Figure 5B).

Immunofluorescence revealed that the assembly of the NADPH oxidase complex on the phagolysosomal membrane was also affected by flotillins (Figure S6). The percentage of phagolysosomes showing assembled NADPH oxidase complex when *pksP* conidia were ingested was reduced from 10% in wild-type macrophages to 2% in $Flot^{-/-}$ BMDMs (Figure 5C). Taken together, deletion of flotillin-encoding genes phenocopied the effect of melanin on phagolysosomes. As shown in Figure 5D, phagocytosis rate of *pksP* conidia was reduced in $Flot^{-/-}$ BMDMs. There was no effect on the phagocytosis rate of wild-type conidia, since these conidia via their DHN-melanin layer most likely already led to reduced flotillins in the membrane forming the phagocytic cup.

FLOT1 SNP Results in Heightened Susceptibility for IA in HSCT Recipients

Our data suggested that flotillin-dependent membrane microdomain formation plays a role in immunity to infection with *A. fumigatus*. To further substantiate this finding, we screened for single-nucleotide polymorphisms (SNPs) and their association with the risk of IA in a cohort of hematopoietic stem cell transplant (HSCT) recipients. For this reason, the donors of hematopoietic stem cells were genotyped. Whereas for the *FLOT2* gene there was no SNP associated with risk of infection, for the *FLOT1* gene, we clearly found a SNP. Based on the haplotype-based tagging strategy applied here, five tagging SNPs were identified in the *FLOT1* gene and genotyped. However, of these, only SNP rs3094127 was associated with an increased risk of IA after stem cell transplantation. The rs3094127 SNP (T > C) is located in the last intron of the human *FLOT1* gene (Figure 6A) and is lacking in the corresponding gene in mice. The cumulative incidence of IA for donor rs309412 was 38.5% for CC ($p = 0.04$), 29.6% for TC ($p = 0.05$), and 19.6% for TT genotypes, respectively (Figure 6B). In a multivariate model accounting for clinical variables associated with or tending toward IA in our cohort, the CC genotype at rs3094127 in *FLOT1* remained an independent predictor of IA (hazard ratio [HR], 1.89; 95% confidence interval [CI], 1.14-5.67; $p = 0.03$). The *FLOT1* genotypes had no impact in overall survival.

To demonstrate a functional effect of the SNP in *FLOT1* on myeloid cell function, we analyzed the responses of monocyte-derived macrophages isolated from healthy genotyped donors. For this purpose, we measured cytokines likely being of relevance for IA, such as interleukin-6 (IL-6) (Cenci et al., 2001), IL-1β (Gresnigt and van de Veerdonk, 2014), IL-10 (Romani, 2011), and tumor necrosis factor alpha (TNF-α) (Garth and Steele, 2017). We found that macrophages from the individuals carrying this SNP produced significantly less IL-1β and IL-6 following *in vitro* stimulation with *A. fumigatus* conidia compared to controls, whereas cytokines TNF-α and IL-10 did not show significant differences (Figure 6C).

DISCUSSION

The lipid microdomains (rafts) hypothesis was originally proposed by Simons and Ikonen (Simons and Ikonen, 1997),

Figure 3. Different Amounts of GM1 Ganglioside and Flot-1 in Conidia-Containing Phagolysosomes

(A) Western blot analysis for detection of caveolin-1 (Cav-1) and caveolin-2 (Cav-2) in RAW264.7 and HeLa cells. GAPDH was used as a control.

(B) Flot-1 and lipid rafts in conidia-containing phagolysosomes. Conidia were stained with CFW (blue), and RAW264.7 macrophages were stained with CTB-Alexa Fluor 647 and an anti-Flotillin-1 antibody (anti-Flot-1) for lipid rafts and Flot-1, respectively. Scale bar, 5 μm.

(C) Channel intensity plot (left) reflecting the CTB and anti-Flot-1 fluorescence signal of the phagolysosomal membrane surrounding the *pksP* conidium (right).

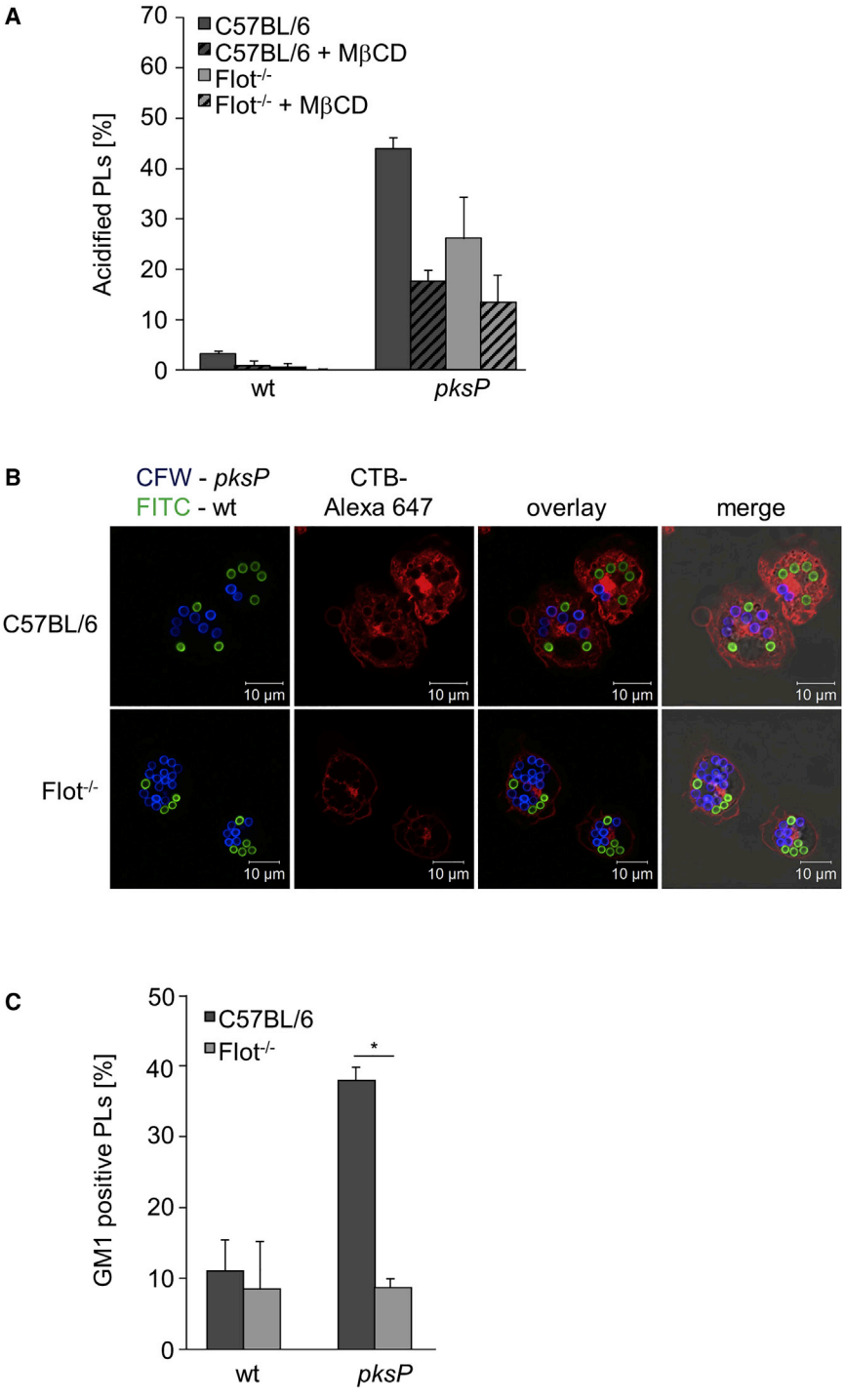

Figure 4. *A. fumigatus* Wild-Type Conidia Interfere with Flotillin-Dependent Formation of Phagolysosomal Lipid Rafts

(A) Quantification of acidified phagolysosomes (PLs) in BMDMs from C57BL/6 or Flot$^{-/-}$ mice. When indicated, MβCD was added. Data are presented as mean ± SD.

(B) Coincubation of BMDMs with wild-type (FITC-labeled, green) and *pksP* (CFW-labeled, blue) conidia. CTB-Alexa Fluor 647 stained GM1 gangliosides (red).

(C) Ratio (in percent) of GM1-positive phagolysosomes (PLs) in BMDMs infected with wild-type and *pksP* conidia. Data are presented as mean ± SD; p = 0.015.

See also Figure S5.

imagining these lipid rafts as floating islands in the membrane. Lipid rafts are defined as small (10–200 nm) heterogeneous, highly dynamic, sterol (cholesterol), sphingolipid- and protein-enriched domains that compartmentalize the cellular processes (Varshney et al., 2016). One of the widely appreciated roles of membrane microdomains is the recruitment of molecules involved in cellular signaling. The formation of a molecular cluster and their signal transduction machinery in membrane rafts leads to enhanced signaling efficiency (Triantafilou et al., 2002). It is thus not surprising that membrane microdomains are required for immunity (Varshney et al., 2016).

Here, we characterized microdomains in the phagolysosomal membrane by using a variety of lipid-raft marker molecules like GM1 ganglioside and cholesterol. To further specify the membrane microdomains, we assessed the localization of typical marker proteins during phagolysosome maturation. Our findings are in accordance with studies underlining that caveolins are not coexpressed in murine macrophages (Gargalovic and Dory, 2001; Martínez-Mármol et al., 2008; Matveev et al., 1999; Nagao et al., 2010). Instead, our data indicate that flotillin-dependent microdomains play a pivotal role in phagosome biogenesis and acidification of phagolysosomes (Lafourcade et al., 2008) and that these membrane structures are targeted by *A. fumigatus* conidia to interfere with the maturation of this compartment. These findings were confirmed by the observation that Flot-1, a marker for a different subset of lipid rafts and assumed to act as scaffolding protein that stabilizes microdomains (Otto and Nichols, 2011; Stuermer, 2011), colocalized with GM1 on phagolysosomal membranes of RAW264.7 cells containing *pksP* conidia, but not melanized conidia. Further, by analyzing knockdown and, more importantly, knockout cells of the flotillin genes, we provide causal evidence that flotillin-dependent membrane microdomains are required for vATPase assembly and NADPH oxidase complex assembly on the phagolysosomal membrane and phagocytosis. Hence, flotillin-dependent membrane microdomains are required for

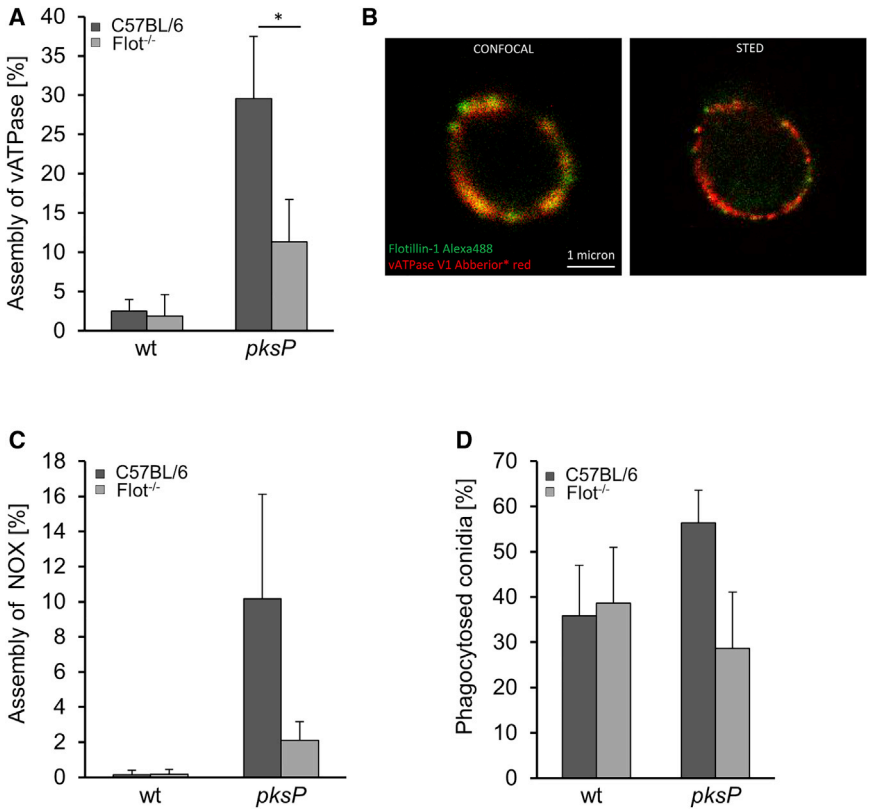

Figure 5. Flotillin-Dependent Lipid Rafts Are Required for vATPase and NADPH Oxidase Assembly and Phagocytosis of Conidia

(A) vATPase assembly in BMDMs isolated from C57BL/6 wild-type and Flot$^{-/-}$ mice measured by immunofluorescence. Data represent mean ± SD; $p < 0.05$.

(B) Colocalization of vATPase and Flot-1. STED microscopy of isolated phagolysosomes stained with anti-Flot-1 and anti-vATPase V_1 antibody.

(C) NADPH oxidase assembly in BMDMs isolated from C57BL/6 and Flot$^{-/-}$ mice measured by immunofluorescence. For vATPase and NADPH oxidase, ≥100 intracellular conidia were evaluated for the presence of a fluorescence signal. The values represent mean ± SD of three independent experiments.

(D) Phagocytosis of conidia by Flot$^{-/-}$ BMDMs. See also Figure S6.

acidification of phagolysosomes, and these findings explain the lack of acidification of phagolysosomes containing wild-type conidia.

Flotillins belong to a family of lipid-raft-associated integral membrane proteins. Flotillin members are ubiquitously expressed and located in non-caveolar microdomains on the cell membrane. Two flotillin members have been described, Flot-1 and Flot-2 (Otto and Nichols, 2011; Vieira et al., 2010). They constitutively associate with lipid rafts by acylation, oligomerization, and cholesterol binding (Meister and Tikkanen, 2014). Consequently, flotillins, either on their own or in combination with the respective other flotillin, have been implicated in numerous signaling events and pathways that are thought to be organized in lipid rafts (Babuke and Tikkanen, 2007). As shown here, by employing BMDMs of Flot$^{-/-}$ mice and knockdown cell lines, microdomains on the phagolysosomal membrane contain and require flotillin proteins.

An important aspect found here is that flotillin-dependent microdomains act as platform for vATPase assembly and NADPH oxidase complex assembly on the phagolysosomal membrane. Further, they contribute to phagocytosis. These findings resulted not only from experiments with knockout cells but also from the colocalization of vATPase and Flot-1 on the phagolysosomal membrane. The reversible binding of the cytoplasmic V_1 complex of vATPase to the V_0 complex in the phagosomal membrane regulates the activity of vATPase (Cotter et al., 2015). Little is known about the role of the vATPase and its regulation associated with the endocytic pathways of immune cells, although this multiprotein complex is crucial for the antimicrobial properties of professional phagocytes (e.g., intracellular killing, digestion, and presentation of antigenic epitopes) (Cotter et al., 2015). Genome-wide knockout studies in *Saccharomyces cerevisiae* showed that the presence of sphingolipids strongly influences the assembly of the vATPase complex (Finnigan et al., 2011). In addition to cholesterol, sphingolipids are key components of lipid rafts (Pike, 2009; Simons and Gerl, 2010). There is a direct link between membrane microdomains and regulation of the vATPase (Dhungana et al., 2009; Lafourcade et al., 2008). Here, by using *Flot-1*/*Flot-2* double-knockout BMDMs and knockdown cell lines, we obtained evidence that the assembly of a functional vATPase on the phagolysosomal membrane requires flotillin-dependent microdomains. In line, by coinfecting macrophages with both wild-type and *pksP* conidia, we observed not only different acidification patterns of phagolysosomes in the same cell but also different localization patterns of the V_1 subunit of the vATPase complex. All of these effects were due to different amounts of microdomains in the phagolysosomal membrane. Thus, dysregulation of phagolysosomal membrane microdomains by melanized conidia is not an overall mechanism of the entire cell but locally restricted to the specific phagolysosomal compartment containing a conidium. These findings correspond with previous results showing that during phagolysosome maturation the association of phagolysosomal compartments with membrane microdomains governs increased acidification due to higher vATPase assembly rates (Lafourcade et al., 2008). The fact that in coinfection assays wild-type and *pksP* conidia induce different membrane microdomain patterns in phagolysosomes present in the same cell also refutes the possibility that the biosynthesis of GM1 or other lipid-raft components is affected by DHN-melanin. It is conceivable, that membrane microdomains are still formed in Flot$^{-/-}$ BMDMs but their stability and their size are reduced

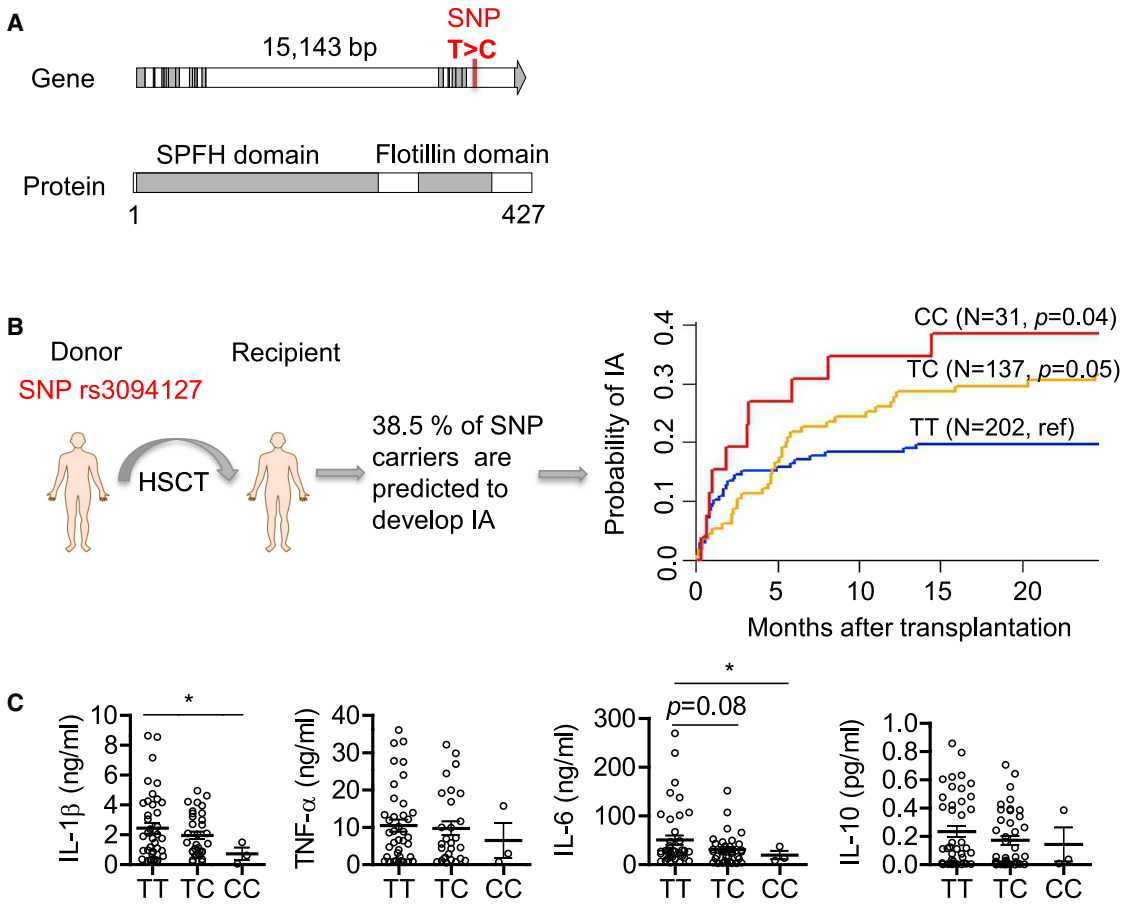

Figure 6. The rs3094127 SNP in *FLOT1* Is Associated with an Increased Risk of IA in Hematopoietic Stem Cell Recipients

(A) Position of SNP found in the human *FLOT1* gene. The SNP changes thymine (T) to cytosine (C).

(B) Cumulative incidence of invasive aspergillosis (IA) in allogeneic HSCT recipients according to donor rs3094127 genotypes in *FLOT1*. Data were censored at 24 months, and relapse and death were competing events. p values are for Gray's test.

(C) Cytokines released by monocyte-derived macrophages obtained from healthy donors with different *FLOT1* genotypes after stimulation with wild-type conidia of *A. fumigatus* for 24 h.

due to the lack of flotillins. This conclusion is also supported by the finding that flotillin-deficient macrophages are still able to acidify *pksP* conidia-containing phagolysosomes albeit with a significant delay compared to wild-type phagocytes. By inducing this delay, the fungus gains time to survive and to escape from the host cell.

As shown for LAP (Kyrmizi et al., 2018), the restriction of the effects to a distinct phagolysosome observed here is most likely due to the binding of activated calmodulin to the phagolysosomal membrane. If free Ca^{2+} can be shuttled from the phagolysosomal lumen to the cytosolic part of the phagosomal membrane, calmodulin on the cytosolic site is activated, and as a result, the phagolysosome is functional, as seen here for phagolysosomes containing *pksP* conidia (Figure 7).

An interesting finding is the dependence of NADPH oxidase complex assembly on flotillin-dependent membrane microdomains. It is conceivable that defects in flotillins result in immune suppression, as shown here in Flot$^{-/-}$ BMDMs phagocytosis, was reduced as well as the number of assembled NADPH oxidase complexes on the phagolysosome membrane. This might lead to reduced production of reactive oxygen species (ROS) that are required for induction of LAP (Martinez et al., 2015). The reduced phagocytosis rate of *pksP* conidia in Flot$^{-/-}$ BMDMs suggests that membrane microdomains are required as signaling platforms for recognition of conidia. By contrast, wild-type conidia did not show different phagocytosis rates because these conidia via their DHN-melanin layer most likely already disturbed flotillins in the membrane forming the phagocytic cup. In line, recently it was shown that Flot-1 facilitates inflammatory Toll-like receptor 3 signaling in human endothelial cells (Fork et al., 2014). The finding that lack of flotillins does not completely inhibit phagolysosomal acidification but significantly delays this process also explains that overall intracellular killing of conidia in Flot$^{-/-}$ BMDMs is not affected after 6 h (data not shown).

Until now, the regulation of membrane microdomain formation is a matter of debate. Here, we found that inhibition of Ca^{2+}-dependent calmodulin activity or melanin-dependent Ca^{2+}

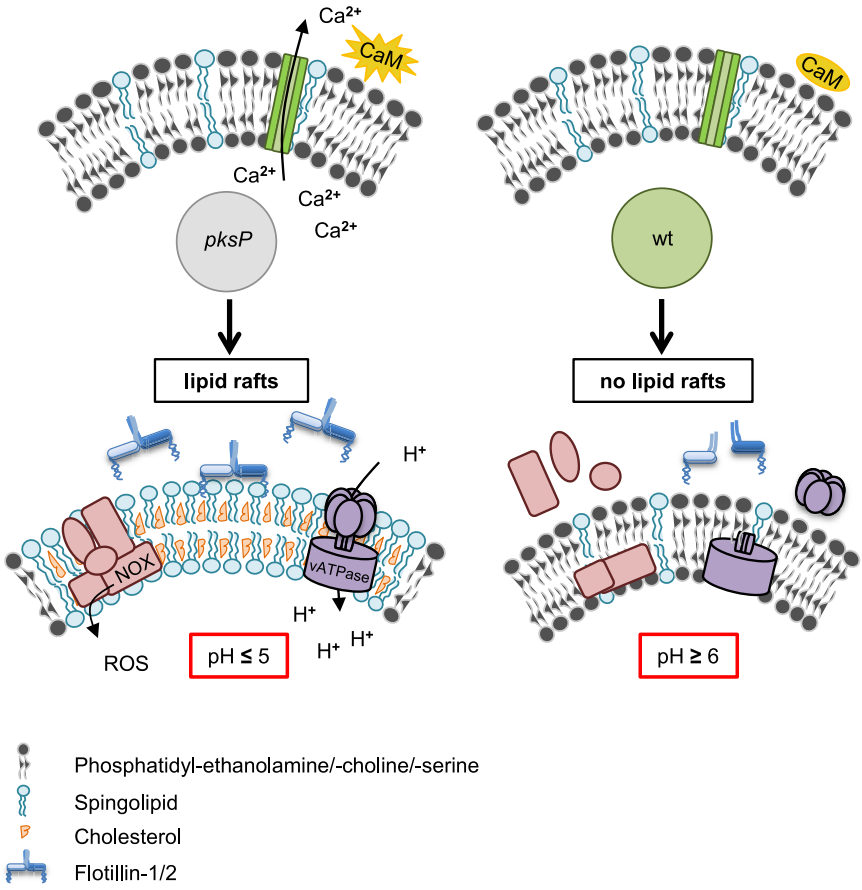

Figure 7. Model Summarizing the Current View
For details, see text.

sequestration in the phagolysosome reduced the presence of microdomains on the phagolysosomal membrane. Calmodulin is a versatile Ca^{2+} sensor/transducer that modulates hundreds of enzymes, channels, transport systems, transcription factors, adaptors, and other structural proteins, controlling in this manner multiple cellular functions. It can regulate target proteins in a Ca^{2+}-dependent or independent manner (Villalobo, 2018). Since we found clear differences in the concentration of free Ca^{2+} in phagolysosomes containing pigmentless conidia versus melanized conidia, these data suggest that the available free Ca^{2+} ions for calmodulin are reduced, and thereby calmodulin activation and membrane microdomain formation are impaired (Figure 7). This conclusion was substantiated by the finding of reduced microdomain formation on the phagolysosomal membrane when cells were treated with a calmodulin inhibitor. Our data well agree with our previous observation that early, transient, and selective calmodulin localization was exclusively observed in phagolysosomes of melanin-deficient conidia (Kyrmizi et al., 2018). At this stage, we can only speculate about the mechanism by which calmodulin potentially regulates the abundance of lipid rafts. Previously, we showed that wild-type conidia inhibit calcium signaling (Kyrmizi et al., 2018). Here, we show that inhibition of Ca^{2+}/calmodulin signaling deregulates lipid-raft formation. Therefore, it is likely that calmodulin is an upstream regulator of lipid-raft formation. In addition, Ca^{2+}/calmodulin plays an important role for fusion of intracellular organelles, including endosomes (Colombo et al., 1997; Di Giovanni et al., 2010). It is thus conceivable that lipid-raft remodeling is connected to fusion events of the phagosome with components of the endocytic pathway. Alternatively, it is also conceivable that the activation of Ca^{2+} channels like distinct transient receptor potential channels (Santoni et al., 2018) in the phagolysosomal membrane require lipid rafts.

Until now, for different pathogens such as viruses, bacteria, and protozoa, it was shown that they can use host cell membrane microdomains to secure their entrance and maintenance inside target cells (Mañes et al., 2003; Vieira et al., 2010). Different viruses have evolved strategies to subvert raft-associated signaling, enabling their efficient replication in immune cells and at the same time blocking the immune response that is elicited by the target cells (Hawkes and Mak, 2006). Likewise, several bacteria interact with host lipid rafts to enter and survive inside the cell (Hawkes and Mak, 2006; Mañes et al., 2003). The mechanisms that underlie this interaction are starting to be unraveled. Activation of secretion, binding, perforation of the host-cell membrane, and signaling to trigger bacterial phagocytosis are involved with components of membrane microdomains (Lafont and van der Goot, 2005; Vieira et al., 2010). In the context of kinase signaling, it was shown that the yeast form of the fungal pathogen *Paracoccidioides brasiliensis* promotes the aggregation of lipid rafts in epithelial cells, allowing fungal adhesion (Maza et al., 2008).

Here, we add a novel virulence mechanism. Unlike many facultative intracellular pathogens, *A. fumigatus* evades phagocytes by impairing lipid-raft formation in phagolysosomal membranes, most likely via Ca^{2+} sequestration by melanized conidia. Thereby, melanized conidia prevent lipid-raft-associated assembly of the signal platforms required (e.g., for assembly of vATPase and NADPH oxidase). However, alternatively, it is also conceivable that incomplete or only partial fusions have occurred between endosomal and lysosomal vesicles instead of complete fusions with entire mixing of the fusion partners' membranes (Desjardins, 1995; Haas, 2007). Since lipid rafts are also associated with functional membrane trafficking (Simons and Gerl, 2010), missing microdomains in the wild-type-conidia-containing phagolysosomal membranes could be responsible for the lack of integration of lysosomal membrane

constituents, which then leads to phagolysosomes devoid of membrane microdomains.

Recently, it was reported that DHN-melanin inhibits the activation of a noncanonical LAP autophagy pathway (Akoumianaki et al., 2016), which is regulated by NADPH oxidase and promotes antifungal defense. It was found that DHN-melanin inhibits NADPH-oxidase-dependent activation of LAP by excluding the p22*phox* subunit from the phagolysosome. Also, NOX2-generated ROS are necessary for LC3 recruitment to phagosomes (Huang et al., 2009). Here, we provide a model explaining that conidial melanin interferes with membrane microdomain formation that is required for NADPH oxidase assembly and most likely all further processes assigned to the activity of melanin (Figure 7).

The importance of the membrane microdomain component flotillin for pathogenicity was further demonstrated by the analysis of hematologic patients undergoing allogeneic HSCT. In human individuals, we identified a SNP in a region of the *FLOT1* gene that is not present in mice and results in heightened susceptibility to IA. Macrophages of individuals homozygous for this SNP showed reduced extracellular amounts of IL-1β and IL-6. IL-1β has been clearly shown to be required for defense against *A. fumigatus* infection (Sainz et al., 2008; Wójtowicz et al., 2015), and flotillin-dependent lipid rafts have been shown to affect cytokine secretion (Kay et al., 2006). For example, the activated dectin-1 receptor, important to sense *A. fumigatus* (Luther et al., 2007; Steele et al., 2005), localizes to lipid-raft microdomains. The receptor has been also shown to be required for signaling and activation of phagocytosis and cytokine production in dendritic cells (Xu et al., 2009). Thus, it is very likely that lipid rafts are required not only for assembly of vATPase but also for activation of receptors and thus for cytokine production. Our data show the functional impairment caused by the SNP and the importance of FLOT1-dependent membrane microdomains for immunity against infections.

As for any intronic SNP, the rs3094127 SNP may act on FLOT1 function via different possible mechanisms, including regulating mRNA expression and/or alternative pre-mRNA splicing. However, we cannot exclude the possibility that this marker influences the risk of IA by being linked with another unknown variant.

Collectively, our data provide new insights into the importance of membrane microdomains for immunity against human pathogenic fungi and as a target for pathogens. Our study adds mechanistic insight into the regulation and formation of membrane microdomains, elucidates a role for microdomain-based signaling in regulation of phagosome biogenesis, and reports a new molecular virulence mechanism via the disruption of membrane microdomains.

Although the recognition of immunological cell wall structures like β-1,3-glucans (Steele et al., 2005), which are more susceptible for receptors on *pksP* conidia (Luther et al., 2007), leads to an activation of immune cells by generation of an inflammatory response through production of chemokines and cytokines (Chai et al., 2010), it does not necessarily result in a higher activation of the endocytic pathway with accompanied acidification of phagolysosomal compartments. This was concluded here from experiments in which the same macrophage had phagocytosed both a wild-type and *pksP* conidium, which, in the same cell, ended in a neutral and acidified phagolysosome, respectively. Instead, each ingested particle determines its intracellular fate via influencing the endocytic pathway by its morphological and chemical properties (in the case of *A. fumigatus* conidia, by the presence or absence of the DHN-melanin layer). Abolishing the phagolysosomal acidification by disturbance of vATPase assembly resulted in increased host cell damage, interestingly to the same extent for both wild-type and *pksP* conidia. Thus, phagolysosomal acidification strongly contributes to the effective killing of conidia (Jahn et al., 2002) and thereby protects the host cell from outgrowth of the ingested pathogen to a certain extent. Inhibition of phagolysosomal acidification and reduction of NADPH oxidase complex assembly by DHN-melanin allows wild-type conidia to create a favorable niche with a nearly neutral pH, which prevents activation of hydrolytic enzymes and thereby phagolysosomal digestion.

STAR★METHODS

Detailed methods are provided in the online version of this paper and include the following:

- KEY RESOURCES TABLE
- RESOURCE AVAILABILITY
  - Lead Contact
  - Materials Availability
  - Data and Code Availability
- EXPERIMENTAL MODEL AND SUBJECT DETAILS
  - Animals
  - Cell lines
  - Human cells
- METHOD DETAILS
  - Cultivation of *A. fumigatus* and staining of conidia
  - Infection experiments
  - Host cell damage assay
  - Immunofluorescence and microscopy
  - Quantitation of phagocytosis, phagolysosomal acidification and recruitment of membrane microdomains
  - Knockdown of flotillin genes
  - Isolation of murine bone marrow-derived macrophages (BMDMs)
  - Extraction and quantification of cholesterol
  - Calcium staining and Calmodulin inhibition
  - Human studies
  - Cytokine measurements
- QUANTIFICATION AND STATISTICAL ANALYSIS

SUPPLEMENTAL INFORMATION

Supplemental Information can be found online at https://doi.org/10.1016/j.celrep.2020.108017.

ACKNOWLEDGMENTS

We are extremely grateful to Ben J. Nichols (Cambridge, UK) for providing flotillin-knockout mice. We thank Maria Straßburger for projecting mouse breeding, Hans-Martin Dahse for cytotoxicity assays, and Matthew Blango for critically reading the manuscript. This work was supported by the International Leibniz Research School (ILRS) as part of the excellence graduate school Jena School for Microbial Communication (JSMC) funded by the

Deutsche Forschungsgemeinschaft (DFG), the Leibniz Science Campus "InfectoOptics," and the DFG-funded CRC 1278 "PolyTarget" (project B02 to A.A.B. and Z01 to M.T.F.). C.C. and A.C were supported by the Northern Portugal Regional Operational Programme (NORTE 2020) under the Portugal 2020 Partnership Agreement, through the European Regional Development Fund (FEDER) (NORTE-01-0145-FEDER-000013), and by the Fundação para a Ciência e Tecnologia (FCT) (SFRH/BPD/96176/2013 to C.C. and IF/00735/2014 to A.C.).

AUTHOR CONTRIBUTIONS

F.S., A.T., M.G., Z.C., H.S., M.R., S.G., A.C., M.H.G., and T.H. conducted experiments and analyzed data. A.A.B., M.T.F., G.C., C.C., A. Carvalho, J.F.L., A. Campos Jr., C.E., and S.G.F. designed research and analyzed data. F.S., H.S., A.T., M.G., T.H., G.C., S.G.F., and A.A.B. wrote the paper.

DECLARATION OF INTERESTS

The authors declare no competing interests.

Received: November 26, 2019
Revised: April 3, 2020
Accepted: July 17, 2020
Published: August 18, 2020

REFERENCES

Akoumianaki, T., Kyrmizi, I., Valsecchi, I., Gresnigt, M.S., Samonis, G., Drakos, E., Boumpas, D., Muszkieta, L., Prevost, M.C., Kontoyiannis, D.P., et al. (2016). *Aspergillus* cell wall melanin blocks LC3-associated phagocytosis to promote pathogenicity. Cell Host Microbe *19*, 79–90.

Andrianaki, A.M., Kyrmizi, I., Thanopoulou, K., Baldin, C., Drakos, E., Soliman, S.S.M., Shetty, A.C., McCracken, C., Akoumianaki, T., Stylianou, K., et al. (2018). Iron restriction inside macrophages regulates pulmonary host defense against *Rhizopus* species. Nat. Commun. *9*, 3333.

Babuke, T., and Tikkanen, R. (2007). Dissecting the molecular function of reggie/flotillin proteins. Eur. J. Cell Biol. *86*, 525–532.

Batanghari, J.W., Deepe, G.S., Jr., Di Cera, E., and Goldman, W.E. (1998). *Histoplasma* acquisition of calcium and expression of CBP1 during intracellular parasitism. Mol. Microbiol. *27*, 531–539.

Bitsikas, V., Riento, K., Howe, J.D., Barry, N.P., and Nichols, B.J. (2014). The role of flotillins in regulating aβ production, investigated using flotillin 1-/-, flotillin 2-/- double knockout mice. PLoS ONE *9*, e85217.

Brown, G.D., Denning, D.W., Gow, N.A., Levitz, S.M., Netea, M.G., and White, T.C. (2012). Hidden killers: human fungal infections. Sci. Transl. Med. *4*, 165rv13.

Cambier, C.J., Falkow, S., and Ramakrishnan, L. (2014). Host evasion and exploitation schemes of *Mycobacterium tuberculosis*. Cell *159*, 1497–1509.

Carvalho, F., Sousa, S., and Cabanes, D. (2014). How *Listeria monocytogenes* organizes its surface for virulence. Front. Cell. Infect. Microbiol. *4*, 48.

Cenci, E., Mencacci, A., Casagrande, A., Mosci, P., Bistoni, F., and Romani, L. (2001). Impaired antifungal effector activity but not inflammatory cell recruitment in interleukin-6-deficient mice with invasive pulmonary aspergillosis. J. Infect. Dis. *184*, 610–617.

Chai, L.Y., Netea, M.G., Sugui, J., Vonk, A.G., van de Sande, W.W., Warris, A., Kwon-Chung, K.J., and Kullberg, B.J. (2010). *Aspergillus fumigatus* conidial melanin modulates host cytokine response. Immunobiology *215*, 915–920.

Colombo, M.I., Beron, W., and Stahl, P.D. (1997). Calmodulin regulates endosome fusion. J. Biol. Chem. *272*, 7707–7712.

Cotter, K., Stransky, L., McGuire, C., and Forgac, M. (2015). Recent insights into the structure, regulation, and function of the V-ATPases. Trends Biochem. Sci. *40*, 611–622.

De Pauw, B., Walsh, T.J., Donnelly, J.P., Stevens, D.A., Edwards, J.E., Calandra, T., Pappas, P.G., Maertens, J., Lortholary, O., Kauffman, C.A., et al.; European Organization for Research and Treatment of Cancer/Invasive Fungal Infections Cooperative Group; National Institute of Allergy and Infectious Diseases Mycoses Study Group (EORTC/MSG) Consensus Group (2008). Revised definitions of invasive fungal disease from the European Organization for Research and Treatment of Cancer/Invasive Fungal Infections Cooperative Group and the National Institute of Allergy and Infectious Diseases Mycoses Study Group (EORTC/MSG) Consensus Group. Clin. Infect. Dis. *46*, 1813–1821.

Dermine, J.F., Duclos, S., Garin, J., St-Louis, F., Rea, S., Parton, R.G., and Desjardins, M. (2001). Flotillin-1-enriched lipid raft domains accumulate on maturing phagosomes. J. Biol. Chem. *276*, 18507–18512.

Desjardins, M. (1995). Biogenesis of phagolysosomes: the 'kiss and run' hypothesis. Trends Cell Biol. *5*, 183–186.

Dhungana, S., Merrick, B.A., Tomer, K.B., and Fessler, M.B. (2009). Quantitative proteomics analysis of macrophage rafts reveals compartmentalized activation of the proteasome and of proteasome-mediated ERK activation in response to lipopolysaccharide. Mol. Cell. Proteomics *8*, 201–213.

Di Giovanni, J., Iborra, C., Maulet, Y., Lévêque, C., El Far, O., and Seagar, M. (2010). Calcium-dependent regulation of SNARE-mediated membrane fusion by calmodulin. J. Biol. Chem. *285*, 23665–23675.

Ensminger, A.W. (2016). *Legionella pneumophila*, armed to the hilt: justifying the largest arsenal of effectors in the bacterial world. Curr. Opin. Microbiol. *29*, 74–80.

Fernández-Arenas, E., Bleck, C.K., Nombela, C., Gil, C., Griffiths, G., and Diez-Orejas, R. (2009). *Candida albicans* actively modulates intracellular membrane trafficking in mouse macrophage phagosomes. Cell. Microbiol. *11*, 560–589.

Filler, S.G., Swerdloff, J.N., Hobbs, C., and Luckett, P.M. (1995). Penetration and damage of endothelial cells by *Candida albicans*. Infect. Immun. *63*, 976–983.

Finnigan, G.C., Ryan, M., and Stevens, T.H. (2011). A genome-wide enhancer screen implicates sphingolipid composition in vacuolar ATPase function in *Saccharomyces cerevisiae*. Genetics *187*, 771–783.

Fork, C., Hitzel, J., Nichols, B.J., Tikkanen, R., and Brandes, R.P. (2014). Flotillin-1 facilitates toll-like receptor 3 signaling in human endothelial cells. Basic Res. Cardiol. *109*, 439.

Frick, M., Bright, N.A., Riento, K., Bray, A., Merrified, C., and Nichols, B.J. (2007). Coassembly of flotillins induces formation of membrane microdomains, membrane curvature, and vesicle budding. Curr. Biol. *17*, 1151–1156.

Gargalovic, P., and Dory, L. (2001). Caveolin-1 and caveolin-2 expression in mouse macrophages. High density lipoprotein 3-stimulated secretion and a lack of significant subcellular co-localization. J. Biol. Chem. *276*, 26164–26170.

Garth, J.M., and Steele, C. (2017). Innate lung defense during invasive Aspergillosis: new mechanisms. j. innate immun. *9*, 271–280.

Gresnigt, M.S., and van de Veerdonk, F.L. (2014). The role of interleukin-1 family members in the host defence against *Aspergillus fumigatus*. Mycopathologia *178*, 395–401.

Haas, A. (2007). The phagosome: compartment with a license to kill. Traffic *8*, 311–330.

Hawkes, D.J., and Mak, J. (2006). Lipid membrane; a novel target for viral and bacterial pathogens. Curr. Drug Targets *7*, 1615–1621.

Heinekamp, T., Thywißen, A., Macheleidt, J., Keller, S., Valiante, V., and Brakhage, A.A. (2013). *Aspergillus fumigatus* melanins: interference with the host endocytosis pathway and impact on virulence. Front. Microbiol. *3*, 440.

Huang, J., Canadien, V., Lam, G.Y., Steinberg, B.E., Dinauer, M.C., Magalhaes, M.A., Glogauer, M., Grinstein, S., and Brumell, J.H. (2009). Activation of antibacterial autophagy by NADPH oxidases. Proc. Natl. Acad. Sci. USA *106*, 6226–6231.

Jahn, B., Koch, A., Schmidt, A., Wanner, G., Gehringer, H., Bhakdi, S., and Brakhage, A.A. (1997). Isolation and characterization of a pigmentless-conidium mutant of *Aspergillus fumigatus* with altered conidial surface and reduced virulence. Infect Immun. *65*, 5110–5117.

Jahn, B., Langfelder, K., Schneider, U., Schindel, C., and Brakhage, A.A. (2002). PKSP-dependent reduction of phagolysosome fusion and intracellular kill of *Aspergillus fumigatus* conidia by human monocyte-derived macrophages. Cell. Microbiol. *4*, 793–803.

Kay, J.G., Murray, R.Z., Pagan, J.K., and Stow, J.L. (2006). Cytokine secretion via cholesterol-rich lipid raft-associated SNAREs at the phagocytic cup. J. Biol. Chem. *281*, 11949–11954.

Kosmidis, C., and Denning, D.W. (2015). The clinical spectrum of pulmonary aspergillosis. Thorax *70*, 270–277.

Kyrmizi, I., Ferreira, H., Carvalho, A., Figueroa, J.A.L., Zarmpas, P., Cunha, C., Akoumianaki, T., Stylianou, K., Deepe, G.S., Jr., Samonis, G., et al. (2018). Calcium sequestration by fungal melanin inhibits calcium-calmodulin signalling to prevent LC3-associated phagocytosis. Nat. Microbiol. *3*, 791–803.

Lafont, F., and van der Goot, F.G. (2005). Bacterial invasion via lipid rafts. Cell. Microbiol. *7*, 613–620.

Lafourcade, C., Sobo, K., Kieffer-Jaquinod, S., Garin, J., and van der Goot, F.G. (2008). Regulation of the V-ATPase along the endocytic pathway occurs through reversible subunit association and membrane localization. PLoS ONE *3*, e2758.

Langfelder, K., Jahn, B., Gehringer, H., Schmidt, A., Wanner, G., and Brakhage, A.A. (1998). Identification of a polyketide synthase gene (pksP) of Aspergillus fumigatus involved in conidial pigment biosynthesis and virulence. Med. Microbiol. Immunol. *187*, 79–89.

Langfelder, K., Streibel, M., Jahn, B., Haase, G., and Brakhage, A.A. (2003). Biosynthesis of fungal melanins and their importance for human pathogenic fungi. Fungal Genet. Biol. *38*, 143–158.

Levitz, S.M., Nong, S.H., Seetoo, K.F., Harrison, T.S., Speizer, R.A., and Simons, E.R. (1999). *Cryptococcus neoformans* resides in an acidic phagolysosome of human macrophages. Infect. Immun. *67*, 885–890.

Lingwood, D., and Simons, K. (2010). Lipid rafts as a membrane-organizing principle. Science *327*, 46–50.

Luther, K., Torosantucci, A., Brakhage, A.A., Heesemann, J., and Ebel, F. (2007). Phagocytosis of *Aspergillus fumigatus* conidia by murine macrophages involves recognition by the dectin-1 beta-glucan receptor and Toll-like receptor 2. Cell. Microbiol. *9*, 368–381.

Maejima, I., Takahashi, A., Omori, H., Kimura, T., Takabatake, Y., Saitoh, T., Yamamoto, A., Hamasaki, M., Noda, T., Isaka, Y., and Yoshimori, T. (2013). Autophagy sequesters damaged lysosomes to control lysosomal biogenesis and kidney injury. EMBO J. *32*, 2336–2347.

Mañes, S., del Real, G., and Martínez-A, C. (2003). Pathogens: raft hijackers. Nat. Rev. Immunol. *3*, 557–568.

Martinez, J., Malireddi, R.K., Lu, Q., Cunha, L.D., Pelletier, S., Gingras, S., Orchard, R., Guan, J.L., Tan, H., Peng, J., et al. (2015). Molecular characterization of LC3-associated phagocytosis reveals distinct roles for Rubicon, NOX2 and autophagy proteins. Nat. Cell Biol. *17*, 893–906.

Martínez-Mármol, R., Villalonga, N., Solé, L., Vicente, R., Tamkun, M.M., Soler, C., and Felipe, A. (2008). Multiple Kv1.5 targeting to membrane surface microdomains. J. Cell. Physiol. *217*, 667–673.

Matveev, S., van der Westhuyzen, D.R., and Smart, E.J. (1999). Co-expression of scavenger receptor-BI and caveolin-1 is associated with enhanced selective cholesteryl ester uptake in THP-1 macrophages. J. Lipid Res. *40*, 1647–1654.

Maza, P.K., Straus, A.H., Toledo, M.S., Takahashi, H.K., and Suzuki, E. (2008). Interaction of epithelial cell membrane rafts with *Paracoccidioides brasiliensis* leads to fungal adhesion and Src-family kinase activation. Microbes Infect. *10*, 540–547.

Mech, F., Thywissen, A., Guthke, R., Brakhage, A.A., and Figge, M.T. (2011). Automated image analysis of the host-pathogen interaction between phagocytes and *Aspergillus fumigatus*. PLoS ONE *6*, e19591.

Meister, M., and Tikkanen, R. (2014). Endocytic trafficking of membrane-bound cargo: a flotillin point of view. Membranes (Basel) *4*, 356–371.

Mohebbi, S., Erfurth, F., Hennersdorf, P., Brakhage, A.A., and Saluz, H.P. (2016). Hyperspectral imaging using intracellular spies: quantitative real-time measurement of intracellular parameters in vivo during interaction of the pathogenic fungus *Aspergillus fumigatus* with human monocytes. PLoS ONE *11*, e0163505.

Nagao, G., Ishii, K., Hirota, K., Makino, K., and Terada, H. (2010). Role of lipid rafts in phagocytic uptake of polystyrene latex microspheres by macrophages. Anticancer Res. *30*, 3167–3176.

Newman, S.L., Gootee, L., Hilty, J., and Morris, R.E. (2006). Human macrophages do not require phagosome acidification to mediate fungistatic/fungicidal activity against *Histoplasma capsulatum*. J. Immunol. *176*, 1806–1813.

Otto, G.P., and Nichols, B.J. (2011). The roles of flotillin microdomains: endocytosis and beyond. J. Cell Sci. *124*, 3933–3940.

Overton, N.L.D., Brakhage, A.A., Thywißen, A., Denning, D.W., and Bowyer, P. (2018). Mutations in EEA1 are associated with allergic bronchopulmonary aspergillosis and affect phagocytosis of *Aspergillus fumigatus* by human macrophages. PLoS ONE *13*, e0185706.

Pike, L.J. (2009). The challenge of lipid rafts. J. Lipid Res. *50* (*Suppl*), S323–S328.

Powers, K.A., Szászi, K., Khadaroo, R.G., Tawadros, P.S., Marshall, J.C., Kapus, A., and Rotstein, O.D. (2006). Oxidative stress generated by hemorrhagic shock recruits Toll-like receptor 4 to the plasma membrane in macrophages. J. Exp. Med. *203*, 1951–1961.

Romani, L. (2011). Immunity to fungal infections. Nat. Rev. Immunol. *11*, 275–288.

Rueden, C.T., Schindelin, J., Hiner, M.C., DeZonia, B.E., Walter, A.E., Arena, E.T., and Eliceiri, K.W. (2017). ImageJ2: ImageJ for the next generation of scientific image data. BMC Bioinformatics *18*, 529.

Sainz, J., Pérez, E., Gómez-Lopera, S., and Jurado, M. (2008). IL1 gene cluster polymorphisms and its haplotypes may predict the risk to develop invasive pulmonary aspergillosis and modulate C-reactive protein level. J. Clin. Immunol. *28*, 473–485.

Santoni, G., Morelli, M.B., Amantini, C., Santoni, M., Nabissi, M., Marinelli, O., and Santoni, A. (2018). "Immuno-transient receptor potential ion channels": the role in monocyte- and macrophage-mediated inflammatory responses. Front. Immunol. *9*, 1273.

Schindelin, J., Arganda-Carreras, I., Frise, E., Kaynig, V., Longair, M., Pietzsch, T., Preibisch, S., Rueden, C., Saalfeld, S., Schmid, B., et al. (2012). Fiji: an open-source platform for biological-image analysis. Nat. Methods *9*, 676–682.

Schmidt, H., Vlaic, S., Krüger, T., Schmidt, F., Balkenhol, J., Dandekar, T., Guthke, R., Kniemeyer, O., Heinekamp, T., and Brakhage, A.A. (2018). Proteomics of *Aspergillus fumigatus* conidia-containing phagolysosomes identifies processes governing immune evasion. Mol. Cell. Proteomics *17*, 1084–1096.

Seider, K., Brunke, S., Schild, L., Jablonowski, N., Wilson, D., Majer, O., Barz, D., Haas, A., Kuchler, K., Schaller, M., and Hube, B. (2011). The facultative intracellular pathogen *Candida glabrata* subverts macrophage cytokine production and phagolysosome maturation. J. Immunol. *187*, 3072–3086.

Simons, K., and Gerl, M.J. (2010). Revitalizing membrane rafts: new tools and insights. Nat. Rev. Mol. Cell Biol. *11*, 688–699.

Simons, K., and Ikonen, E. (1997). Functional rafts in cell membranes. Nature *387*, 569–572.

Skowyra, M.L., Schlesinger, P.H., Naismith, T.V., and Hanson, P.I. (2018). Triggered recruitment of ESCRT machinery promotes endolysosomal repair. Science *360*, eaar5078.

Smith, L.M., Dixon, E.F., and May, R.C. (2015). The fungal pathogen *Cryptococcus neoformans* manipulates macrophage phagosome maturation. Cell. Microbiol. *17*, 702–713.

Solis, G.P., Hoegg, M., Munderloh, C., Schrock, Y., Malaga-Trillo, E., Rivera-Milla, E., and Stuermer, C.A. (2007). Reggie/flotillin proteins are organized into stable tetramers in membrane microdomains. Biochem. J. *403*, 313–322.

Stappers, M.H.T., Clark, A.E., Aimanianda, V., Bidula, S., Reid, D.M., Asamaphan, P., Hardison, S.E., Dambuza, I.M., Valsecchi, I., Kerscher, B., et al. (2018). Recognition of DHN-melanin by a C-type lectin receptor is required for immunity to *Aspergillus*. Nature *555*, 382–386.

Steele, C., Rapaka, R.R., Metz, A., Pop, S.M., Williams, D.L., Gordon, S., Kolls, J.K., and Brown, G.D. (2005). The beta-glucan receptor dectin-1 recognizes specific morphologies of *Aspergillus fumigatus*. PLoS Pathog. *1*, e42.

Stuermer, C.A. (2011). Microdomain-forming proteins and the role of the reggies/flotillins during axon regeneration in zebrafish. Biochim. Biophys. Acta *1812*, 415–422.

Thiele, D.L., and Lipsky, P.E. (1990). Mechanism of L-leucyl-L-leucine methyl ester-mediated killing of cytotoxic lymphocytes: dependence on a lysosomal thiol protease, dipeptidyl peptidase I, that is enriched in these cells. Proc. Natl. Acad. Sci. USA *87*, 83–87.

Thywißen, A., Heinekamp, T., Dahse, H.M., Schmaler-Ripcke, J., Nietzsche, S., Zipfel, P.F., and Brakhage, A.A. (2011). Conidial dihydroxynaphthalene melanin of the human pathogenic fungus *Aspergillus fumigatus* interferes with the host endocytosis pathway. Front. Microbiol. *2*, 96.

Triantafilou, M., Miyake, K., Golenbock, D.T., and Triantafilou, K. (2002). Mediators of innate immune recognition of bacteria concentrate in lipid rafts and facilitate lipopolysaccharide-induced cell activation. J. Cell Sci. *115*, 2603–2611.

Tucker, S.C., and Casadevall, A. (2002). Replication of *Cryptococcus neoformans* in macrophages is accompanied by phagosomal permeabilization and accumulation of vesicles containing polysaccharide in the cytoplasm. Proc. Natl. Acad. Sci. USA *99*, 3165–3170.

Varshney, P., Yadav, V., and Saini, N. (2016). Lipid rafts in immune signalling: current progress and future perspective. Immunology *149*, 13–24.

Vieira, F.S., Corrêa, G., Einicker-Lamas, M., and Coutinho-Silva, R. (2010). Host-cell lipid rafts: a safe door for micro-organisms? Biol. Cell *102*, 391–407.

Villalobo, A. (2018). The multifunctional role of phospho-calmodulin in pathophysiological processes. Biochem. J. *475*, 4011–4023.

Volling, K., Thywissen, A., Brakhage, A.A., and Saluz, H.P. (2011). Phagocytosis of melanized *Aspergillus* conidia by macrophages exerts cytoprotective effects by sustained PI3K/Akt signalling. Cell. Microbiol. *13*, 1130–1148.

Wójtowicz, A., Gresnigt, M.S., Lecompte, T., Bibert, S., Manuel, O., Joosten, L.A., Rüeger, S., Berger, C., Boggian, K., Cusini, A., et al.; Swiss Transplant Cohort Study (STCS); Swiss Transplant Cohort Study STCS (2015). IL1B and DEFB1 polymorphisms increase susceptibility to invasive mold infection after solid-organ transplantation. J. Infect. Dis. *211*, 1646–1657.

Xu, S., Huo, J., Gunawan, M., Su, I.H., and Lam, K.P. (2009). Activated dectin-1 localizes to lipid raft microdomains for signaling and activation of phagocytosis and cytokine production in dendritic cells. J. Biol. Chem. *284*, 22005–22011.

Zaragoza, O., Chrisman, C.J., Castelli, M.V., Frases, S., Cuenca-Estrella, M., Rodríguez-Tudela, J.L., and Casadevall, A. (2008). Capsule enlargement in *Cryptococcus neoformans* confers resistance to oxidative stress suggesting a mechanism for intracellular survival. Cell. Microbiol. *10*, 2043–2057.

Zhang, X., Goncalves, R., and Mosser, D.M. (2008). The isolation and characterization of murine macrophages. Curr. Protoc. Immunol. *Chapter 14*, Unit 14.11.

STAR★METHODS

KEY RESOURCES TABLE

REAGENT or RESOURCE	SOURCE	IDENTIFIER
Chemicals		
20x NuPAGE MES Puffer	Invitrogen	NP0002
2-Mercapthoethanol	GIBCO	3130010
4x NuPage LDS loading buffer	Invitrogen	NP0007
ACK lysis buffer	GIBCO	A1049201
Alexa Fluor 647-conjugated Cholera Toxin B	Life Technologies	C34778
anti-$CD14^+$ coated beads	Miltenyi Biotech	130-050-201
Bafilomcyin A1	Abcam	ab120497
Bovine serum albumin	AppliChem	A1391.0500
Calcofluor white	Sigma-Aldrich	18909
Calmodulin inhibitor W7	Sigma-Aldrich	A3281
CheLuminate-HRP PicoDetect	AppliChem	A3417,1200
Cholesterol	Sigma-Aldrich	C8667
DMEM	GIBCO	11960044
DMSO	VWR	1029500500
Fetal bovine serum	GE Healthcare Life Sciences	SV30160.03.
Fluo-4	Life Technologies	F10473
Fluorescein isothiocyanate	Sigma-Aldrich	F7250
Gentamicin sulfate	GIBCO	15750060
GM-CSF	Miltenyi Biotec	130-093-862
HEPES (1M)	GIBCO	15630056
Histopaque®-1077	Sigma-Aldrich	10771
Human serum	Sigma-Aldrich	H3667
Lipofectamin 2000	Life Technologies	11668019
L-Leucine methyl ester hydrochloride (LLOMe)	Sigma-Aldrich	L1002
LysoTracker Red DND-99	Life Technologies	L7528
M-CSF	Peprotech	315-02
Methyl-β-cyclodextrin	Sigma-Aldrich	C4555
Normal goat serum	Invitrogen	01-6201
N-pentadecanoyl-D-*erythro*-sphingosine	Biotrend	2037
pHRodo	Invitrogen	P36011
RPMI-1640	GIBCO	21875034
siRNA	Santa Cruz Biotechnology	N/A
Sodium bicarbonate	GIBCO	25080094
Sodium dodecyl sulfate	Merck	817034
Ultraglutamine	GIBCO	35050061
Antibodies		
primary		
Rabbit anti-ATP6V1B2	Abcam	ab73404; RRID:AB_1924799
Rabbit anti-p47*phox*	Santa Cruz Biotechnology	sc-14015; RRID:AB_2150289
Rabbit anti-Flotillin-1	Santa Cruz Biotechnology	sc-25506; RRID:AB_2106567
Goat anti-Flotillin-1	Abcam	ab13493; RRID:AB_2294271
Mouse anti-Flotillin-1	BD Biosciences	610820; RRID:AB_398139
Mouse anti-Flotillin-2	BD Biosciences	610384; RRID:AB_610384

(*Continued on next page*)

Continued

REAGENT or RESOURCE	SOURCE	IDENTIFIER
Rabbit anti-Caveolin-1	Cell Signaling Technology	3267; RRID:AB_2275453
Rabbit anti-Caveolin-2	Abcam	ab133484
Rabbit anti-GAPDH	Cell Signaling Technology	2118; RRID:AB_561053
Rabbit anti-CHMP4B	Abcam	ab105767; RRID:AB_10858466
Rabbit anti-Galectin 3	Santa Cruz Biotechnology	sc-515582
secondary		
Goat anti-rabbit Alexa Fluor 647	Cell Signaling Technology	4414; RRID:AB_10693544
Goat anti-rabbit IgG DyLight 633	Thermo Fisher Scientific	35562; RRID:AB_1307539
Goat anti-rabbit Abberior Star Red	Abberior GmbH	STRED; RRID:AB_2833015
Goat anti-rabbit Alexa Fluor 555	Life Technologies	A-21430; RRID:AB_10374475
Donkey anti-goat Alexa Fluor 488	Life Technologies	A-11055; RRID:AB_2534102
Goat anti-rabbit IgG-HRP	Santa Cruz Biotechnology	sc-2054; RRID:AB_631748
anti-mouse IgG-HRP	Cell Signaling Technology	7076; RRID:AB_330924
Critical Commercial Assays		
CellTiter-Blue® Cell Viability assay	Promega	G8080
Qproteome Cell Compartment Kit	QIAGEN	37502
2-D Quant Kit	GE Healthcare	80648356
ELISA MAX^{TM} Deluxe Set Human IL-1β	BioLegend	437004
ELISA MAX^{TM} Deluxe Set Human IL-6	BioLegend	430504
ELISA MAX^{TM} Deluxe Set Human IL-10	BioLegend	430604
ELISA MAX^{TM} Deluxe Set Human TNFα	BioLegend	430204
KASPar assay	LGC Genomics	https://www.biosearchtech.com
Experimental Models: Cell lines		
MH-S	ATCC	ATCC:CRL-2019
J774A.1	ATCC	ATCC:TIB-67
HeLa	ATCC	ATCC:CCL-2
RAW264.7	ATCC	ATCC:TIB-71
Experimental Models: Organisms/Strains		
Aspergillus fumigatus strain ATTCC46645	ATCC	ATCC:46645
Aspergillus fumigatus strain ATTCC46645 *pksP*	Jena Microbial Resource Collection (JMRC), HKI Jena	(Langfelder et al., 1998)
Flot$^{-/-}$ mice (male)	Ben J. Nichols (Cambridge, UK)	(Bitsikas et al., 2014)
C57BL/6J mice (male)	Service Unit Experimental Biomedicine of the University Hospital Jena, Jena, Germany	N/A
Software		
Custom-written Fiji macro, based on the ImageJ version 1.51w	N/A	https://fiji.sc; (Schindelin et al., 2012)
Imaris 8.4.1	Bitplane AG	https://imaris.oxinst.com
Quantity One	Bio-Rad	https://www.bio-rad.com
Analyst 1.4	Sciex	https://sciex.com
Zeiss ZEN software 2.3	Zeiss	http://www.zeiss.de/

RESOURCE AVAILABILITY

Lead Contact

Further information and requests for resources and reagents should be directed to and will be fulfilled by the Lead Contact, Axel A. Brakhage (axel.brakhage@leibniz-hki.de)

Materials Availability

Any material generated in this study are available from the Lead Contact with a completed Materials Transfer Agreement.

Data and Code Availability

This study did not generate any unique datasets or code.

EXPERIMENTAL MODEL AND SUBJECT DETAILS

Animals

Flot$^{-/-}$ mice (Bitsikas et al., 2014) were a kind gift of Ben J. Nichols (Cambridge, UK). C57BL/6J mice (8-9 weeks old) were supplied by Charles River (Sulzfeld, Germany). Breeding service of Flot$^{-/-}$ mice and C57BL/6J mice was provided by the Service Unit Experimental Biomedicine of the University Hospital Jena, Germany. For experiments, only male mice were used. All animals were cared for in accordance with the European animal welfare regulation and approved by the responsible federal/state authority and ethics committee in accordance with the German animal welfare act (permit no. 03-072/16).

Cell lines

MH-S (ATCC:CRL-2019), J774A.1 (ATCC:TIB-67), HeLa (ATCC:CCL-2) and RAW264.7 cells (ATCC:TIB-71) were cultivated in RPMI 1640 or DMEM, respectively, at 37°C, 5 % (v/v) CO_2 in a humidified chamber. DMEM media were supplemented with 10% (v/v) FBS, 1% (w/v) ultraglutamine and 27.5 μg/ml gentamicin sulfate. RPMI 1640 was supplemented with 10% (v/v) FBS, 1% (w/v) ultraglutamine, 1 % (w/v) sodium bicarbonate and 0.05 M 2-mercapthoethanol.

Human cells

Peripheral blood mononuclear cells (PBMCs) were enriched from buffy coats or whole blood by density gradient using Histopaque®-1077, washed twice in PBS and resuspended in RPMI-1640 culture medium with 2 mM glutamine supplemented with 10 % (v/v) human serum, 10 U/ml penicillin/streptomycin and 10 mM HEPES (cRPMI). Monocytes were then isolated from PBMCs using positive magnetic bead separation with anti-CD14$^+$ coated beads according to the manufacturer's instructions. Isolated monocytes were resuspended in cRPMI medium and seeded at a concentration of 1 × 10^6 cells/ml in 24-well plates and 96-well plates (Corning Inc.) and 8 well chamber slides w/cover RS Glass slide sterile (LAB-TEK, Thermo Fisher Scientific) for 7 days in the presence of 20 ng/ml recombinant human granulocyte macrophage colony-stimulating factor (GM-CSF) or 20 ng/ml of macrophage colony-stimulating factor (M-CSF). The culture medium was replaced every 3 days and acquisition of macrophage morphology was confirmed by visualization in an inverse microscope.

METHOD DETAILS

Cultivation of *A. fumigatus* and staining of conidia

The *A. fumigatus* strains used in this study, the ATCC46645 wild-type and the non-pigmented *pksP* mutant, were cultivated on *Aspergillus* minimal medium (AMM) agar plates as described elsewhere (Jahn et al., 1997). Conidia were harvested and labeled with Calcofluor White (CFW) and fluorescein isothiocyanate (FITC) as previously described (Thywißen et al., 2011).

Infection experiments

For infection experiments, macrophages were seeded in 24 well plates with or without glass coverslips at a density of 3 × 10^5 cells per well for microscopic analysis. For post-infection subcellular fractionation 4 × 10^6 cells per well were seeded in 4 well plates. Fluorescence-labeled or non-stained conidia were added at a multiplicity of infection (MOI) of 2, 4 or 5. Synchronization of infection was achieved by centrifugation for 5 min at 100 x *g*. Infection was allowed to proceed for 30 min or 2 h at 37°C in a humidified chamber at 5 % (v/v) CO_2. The coincubation samples were processed afterward according to the requirements of the respective assay.

Host cell damage assay

Host cell damage caused by *A. fumigatus* was measured by the previously described ^{51}Cr release assay (Filler et al., 1995). Briefly, RAW264.7, seeded with a concentration of 3 × 10^5 cells per well in a 25 well plate were loaded with 6 μCi/ml $Na_2{}^{51}CrO_4$ overnight. After removing the unincorporated ^{51}Cr, the cells were infected at an MOI = 2 in the presence or absence of 10 nM bafilomycin A1 with 0.01 % (v/v) DMSO as solvent control. After incubation for 24 h, the amount of ^{51}Cr released to the supernatant and retained by the host cells was determined by γ-counting. Wells containing only host cells were processed in parallel to determine the spontaneous release of ^{51}Cr.

Immunofluorescence and microscopy

After infection and respective coincubation time, cells were fixed for 15 min with 3.7 % (v/v) formaldehyde or cold methanol/aceton at an 80:20 ratio, membranes were permeabilized for 10 min with 0.1 %(v/v) Triton X-100/PBS and blocked for 30min with 5% (v/v) normal goat serum, 1 % (w/v) BSA, 0.3 M glycine/PBS before incubation with primary anti-ATP6V1B2 antibody in 1 % (w/v) BSA/PBS,

followed by incubation with secondary goat anti-rabbit-Alexa Fluor 647 antibody or goat anti-rabbit IgG secondary antibody DyLight 633. For STED microscopy the antibody goat anti-rabbit Abberior Star Red was used. For immunofluorescence of p47*phox* the goat anti-rabbit IgG secondary antibody DyLight 633 was used. To quantify vATPase or NOX assembly, phagolysosomes with a positive signal for ATP6V1B2 or p47*phox* were counted and related to non-stained phagolysosomes. For immunofluorescence of Flot-1 the secondary antibody was goat anti-mouse Alexa Fluor 555 or donkey anti-goat-Alexa Fluor 488. Samples were visualized using a Zeiss LSM 780 confocal microscope and processed with the Zeiss ZEN software. STED images were performed at a Leica SP8 STED microscope. The microscope provides 488 nm and 633 nm excitation lines and 592 nm and 775 nm depletion beams, respectively. The beams are focused into the sample via a 100x/1.4 (Leica HC PL APO) oil immersion objective lens and the detected fluorescence is split onto detectors depending on the characteristic emission wavelengths. Image acquisition was done frame by frame with 23 nm pixel size.

Antibodies			
primary			
Rabbit anti-ATP6V1B2	Abcam	ab73404	1: 200
Rabbit anti-p47*phox*	Santa Cruz Biotechnology	sc-14015	1:100
Rabbit anti-Flotillin-1	Santa Cruz Biotechnology	sc-25506	1:100
Goat anti-Flotillin-1	Abcam	ab13493	1:200
Rabbit anti-CHMP4B	Abcam	ab105767	1:100
Rabbit anti-Galectin 3	Santa Cruz Biotechnology	sc-515582	1:100
secondary			
Goat anti-rabbit Alexa Fluor 647	Cell Signaling Technology	4414	1:500
Goat anti-rabbit IgG DyLight 633	Thermo Fisher Scientific	35562	1:200 to 1:500
Goat anti-rabbit Abberior Star Red	Abberior GmbH	STRED	1:100
Goat anti-mouse Alexa Fluor 555	Life Technologies	A21430	1:100
Donkey anti-goat Alexa Fluor 488	Life Technologies	A11055	1:200

Quantitation of phagocytosis, phagolysosomal acidification and recruitment of membrane microdomains

To determine phagocytosis of macrophages, cells were infected with fluorescein isothiocyanate (FITC)-labeled conidia of *A. fumigatus* at a 1:5 effector-to-target ratio for 30 min, Phagocytosis was stopped by washing wells with cold PBS and extracellular conidia were stained with 0.25 mg/mL Calcofluor White for 15 min. Wells were then washed twice with PBS and cells were fixed with 3.7 % (v/v) formaldehyde/PBS for 15 min. Two hundred phagocytosed conidia were counted and compared to the number of non-phagocytosed conidia. To determine phagolysosmal acidification macrophages were preloaded with 50 nM LysoTracker Red DND-99 in medium for 1 h in the absence or presence of methyl-β-cyclodextrin (MβCD) prior to infection. Cytotoxic effects of different MβCD concentrations were evaluated by the Resazurin-based CellTiter-Blue® Cell Viability assay. For further experiments, we used a concentration of 7.5 mM MβCD that was also applied before (Powers et al., 2006) and that had no major effect on the viability of RAW264.7 macrophages (Figure S7), although other not easily detectable effects on the cells cannot be excluded. Macrophages were infected with an MOI = 2 of *A. fumigatus* wildtyp (ATCC46645) or *pksP* mutant conidia or coinfected with an MOI = 4. To further evaluate phagolysosomal acidification conidia of wt or *pksP* strain were labeled with 0.1 mg/ml phRodo (Invitrogen, P36011), dissolved in DMSO, and conicubated with RAW264.7 cells (MOI = 2) for 2 h. Visualization of GM1 gangliosides was done as follows: After addition of 1.5 μM Alexa Fluor 647-conjugated Cholera Toxin B (CTB), cells were infected with *A. fumigatus* conidia as described above. Phagocytosis was allowed to proceed for 2 h. Then, fixed cells were subjected to microscopical analysis. For the colocalization experiment one hundred conidia-containing phagolysosomes were counted and evaluated for acidification and recruitment of membrane microdomains due to the ganglioside GM1. The values represent mean ± SD of three different experiments. The automated image analysis was carried out by a custom-written Fiji macro, based on the ImageJ version 1.51w. Here the images were despeckled in order to remove salt-and-pepper noise, followed by blurring with a Gaussian filter of 2 pixels width. The background and foreground pixels were separated automatically by the Triangle algorithm. The foreground pixels were binarized and morphologically filtered (dilation by one pixel, hole filling, and erosion by one pixel). The resulting binary objects were separated into regions of interest by applying the Find Particles tool in Fiji, at the same time applying size and shape filtering in order to select only those objects that corresponded to phagolysosomes. The selected regions were used to measure the fluorescence intensity of individual phagolysosomes in the original confocal microscopy images. The results were exported as CSV for statistical analysis and plotting. In order to generate the videos of microdomains surrounding conidia, the confocal image stacks were processed by the software Imaris 8.4.1 using the Zeiss native image file format in order to render the spores and the microdomains as 3D surfaces. The comparison of

phagocytosed wild-type and *pksP* conidia was performed by maintaining the same rendering conditions for both fluorescence channels during the image processing workflow. This included the selection of the fluorescence threshold values, as well as the scale of smoothing for both channels. The green and red rendered surfaces were finally co-plotted in the surface mode of Imaris and rotated in 3D in order to produce an easily interpretable animation (see supplementary Videos S1 and S2) of the relative localization of the spores and membrane microdomains. To further substantiate lipid microdomains macrophages were treated with 3 μl/ml lipophilic dye DiD in culture medium for 20 min, 37°C, 5 % (v/v) CO_2 prior to infection.

Antibodies			
primary			
Rabbit anti-ATP6V1B2	Abcam	ab73404	1:1000
Mouse anti-Flotillin-1	BD Biosciences	610820	1:1000
Mouse anti-Flotillin-2	BD Biosciences	610384	1:1000
Rabbit anti-Caveolin-1	Cell Signaling Technology	3267	1:1000
Rabbit anti-Caveolin-2	Abcam	ab133484	1:1000
Rabbit anti-GAPDH	Cell Signaling Technology	2118	1:2000
secondary			
anti-rabbit IgG-HRP	Santa Cruz Biotechnology	sc-2054	1:1000 to 1:2000
anti-mouse IgG-HRP	Cell Signaling Technology	7076	1:2000

Knockdown of flotillin genes

J774A.1 cells were seeded with a density of 3×10^5 or 1×10^5 in 6-well or 24-well plates in DMEM supplemented with 10 % (v/v) FBS and 1 % (w/v) ultraglutamine. After 24 hours the cells were transfected with 40 nM target specific siRNA and 3-6 μl Lipofectamin 2000. To avoid precipitation of the loaded cationic micelles, medium without FBS and antibiotics was used. After 24 h, medium was changed to DMEM, including supplements. To verify the knockdown of flotillins, samples from different time points were analyzed by immunoblotting. As primary antibodies, anti-Flotillin-1 and anti-Flotillin-2 were used; as secondary antibody anti-mouse IgG-HRP antibody was applied.

Isolation of murine bone marrow-derived macrophages (BMDMs)

Bone marrow cells were isolated from femurs and tibias of specific pathogen-free male mice with an age of 12 to 14 weeks according to a procedure described elsewhere (Zhang et al., 2008). Lysis of red blood cells was achieved by treatment with ACK lysis buffer. BMDMs were differentiated by cultivation of bone marrow cells for at least 5 d in DMEM supplemented with macrophage colony-stimulating factor (M-CSF), 10 % (v/v) FBS, 1 % (w/v) ultraglutamine and 0.05 M 2-mercaptoethanol.

Extraction and quantification of cholesterol

Cholesterol measurements were performed using liquid chromatography coupled to triple-quadrupole mass spectrometry (LC-MS/MS). Adherent cells were treated for 15 min with 1 mL methanol on ice, and the methanol phase was transferred into glass centrifuge tubes. After addition of the internal standard (N-pentadecanoyl-D-*erythro*-sphingosine, 300 pmol/sample, Matreya LLC) samples were mixed with 200 μL 6 N hydrochloric acid and 1 mL PBS and vigorously vortexted for 10 min in the presence of 2 mL chloroform. Aqueous and chloroform phases were separated by centrifugation for 3 min at 1900 x *g*, and the lower chloroform phase was transferred into a new glass centrifuge tube. After a second round of lipid extraction with additional 2 mL chloroform, the two chloroform phases were combined and vacuum-dried at 50°C for 50 min using a vacuum concentrator. The extracted lipids were dissolved in 100 μL methanol/chloroform (4:1, v/v) and stored at −20°C. Detection was performed with the QTrap triple-quadrupole mass spectrometer (Sciex) interfaced with the Merck-Hitachi Elite LaChrom chromatograph and autosampler (VWR, Dresden, Germany). Positive atmospheric pressure chemical ionization (APCI) LC-MS/MS analysis was used for detection of all analytes. The ion source conditions and gas settings for positive APCI LC-MS/MS analysis were as follows: Needle current 4 μA, ion source heater temperature 450°C, collision gas setting medium, ion source gases 1 and 2 settings 30 psi and 15 psi, respectively, curtain gas setting 45 psi. Multiple reaction monitoring (MRM) transitions were as follows: N-pentadecanoyl-D-*erythro*-sphingosine m/z 524/264 $[M + H]^+$, cholesterol m/z 369/95 $[M + H - H_2O]^+$. Liquid chromatographic resolution of all analytes was achieved using a 2x60 mm MultoHigh C18 reversed phase column with 3 μm particle size (CS-Chromatographie Service). The column was equilibrated with 10 % (v/v) methanol and 90 % of 1 % (v/v) formic acid in H_2O for 10 min, followed by sample injection and 25 min elution with 100 % (v/v) methanol with a flow rate of 300 μl/min. Standard curves were generated by adding increasing concentrations of the analytes to 300 pmol of the internal standard. Linearity of the standard curves and correlation coefficients were obtained by linear regression analyzes. Data analyzes were performed using Analyst 1.4.

Calcium staining and Calmodulin inhibition

Cells were loaded at a 1:1 ratio of Fluo-4 and cell medium (DMEM) 30 min before coincubation. After infection with conidia (MOI = 5) cells were coincubated for 2 h and phagolysosomes were isolated as described before. The calmodulin inhibitor W7 was used with a concentration of 10 μM and was added 10 min before infection with FITC-labeled conida respective MOI = 2. After coincubation for 2 h the acidification or lipid raft recruiment represented by GM1 was done like described above. The calcium-sensitive fluorescence intensity analysis was carried out with a custom-written macro in Fiji built on ImageJ 1.52 s (Rueden et al., 2017; Schindelin et al., 2012). The comparison of wild-type conidia-containing phagolysosomes and *pksP* conidia-containig phagolysosomes was done considering the same thresholds as well as filter settings for size and/or shape.

Human studies

A total of 370 hematologic patients undergoing allogeneic hematopoietic stem-cell transplantation at the Hospital of Santa Maria, Lisbon and Instituto Português de Oncologia (IPO), Porto, between 2009 and 2014 were enrolled in the study (Stappers et al., 2018), including 79 cases of probable/proven aspergillosis and 244 uninfected controls. The cases of invasive aspergillosis were identified and classified as 'probable' or 'proven' according to the revised standard criteria from the European Organization for Research and Treatment of Cancer/Mycology Study Group (EORTC/MSG) (De Pauw et al., 2008). Study approval for the genetic association study was obtained from the Ethics Subcommittee for Life and Health Sciences of the University of Minho, Portugal (125/014), the Ethics Committee for Health of the Instituto Português de Oncologia - Porto, Portugal (26/015), the Ethics Committee of the Lisbon Academic Medical Center, Portugal (632/014), and the National Commission for the Protection of Data, Portugal (1950/015). Functional studies on human cells were approved by Ethics Subcommittee for Life and Health Sciences of the University of Minho, Portugal (SECVS-014/2015). All individuals provided written informed consent in accordance with the Declaration of Helsinki. Genomic DNA was isolated from whole blood using the QIAcube automated system (QIAGEN). SNPs were selected using a haplotype-based tagging strategy, in which SNPs were selected based on their ability to tag surrounding variants with a pairwise correlation coefficient r2 of at least 0.80 and a minor allele frequency $\geq$ 5 % using publically available sequencing data from the Pilot 1 of the 1000 Genomes Project for the CEU population. Using these criteria, five tagging SNPs were identified and genotyped. Out of these, only SNP rs3094127 provided a significant association with invasive aspergillosis after stem-cell transplantation. All clinical and genetic variables achieving a p value $\leq$ 0.15 in the univariate analysis were entered one by one in a pairwise model together and kept in the final model if they remained significant (p <0.05). Multivariate analysis was performed using the subdistribution regression model of Fine and Gray with the cmprsk package for R. Therefore, despite the testing of five different SNPs, the only genetic variable added to the model was the rs3094127 genotype. In addition, the demographic and clinical variables tested were age and gender, underlying diseases, type of donor, acute GVHD grades III and IV, and antifungal prophylaxis. Genotyping of the rs3094127 SNP in the *FLOT1* gene was performed using KASPar assays (LGC Genomics) in an Applied Biosystems 7500 Fast PCR system (Thermo Fisher).

Cytokine measurements

MDMs (5×10^5/well in 24-well plates) were infected with *A. fumigatus* conidia at a 1:10 effector-to-target ratio for 24 h at 37°C and 5% (v/v) CO_2. After infection, supernatants were collected and cytokine levels were quantified using ELISA MAX Deluxe Set kits (BioLegend) for human IL-1β, IL-6, IL-10 and TNF-α, according to the manufacturer's instructions.

QUANTIFICATION AND STATISTICAL ANALYSIS

Data are presented as mean ± SD. If not stated otherwise, at least 100 events per sample of three biological replicates in total were quantified. p values were calculated by a one-way ANOVA (Bonferroni's post hoc test). For single comparison, p values were calculated by a two-tailed Student's t test. To assess the statistical significance of a prognostic factor in a cumulative incidence analysis the Gray's test function incorporated in the cmprsk package of R was selected. All statistical analyses were performed using GraphPad Prism Version 6. Statistical details of experiments can be found in the figure legends.

Cell Reports, Volume *32*

Supplemental Information

Flotillin-Dependent Membrane Microdomains Are Required for Functional Phagolysosomes against Fungal Infections

Franziska Schmidt, Andreas Thywißen, Marie Goldmann, Cristina Cunha, Zoltán Cseresnyés, Hella Schmidt, Muhammad Rafiq, Silvia Galiani, Markus H. Gräler, Georgios Chamilos, João F. Lacerda, António Campos Jr., Christian Eggeling, Marc Thilo Figge, Thorsten Heinekamp, Scott G. Filler, Agostinho Carvalho, and Axel A. Brakhage

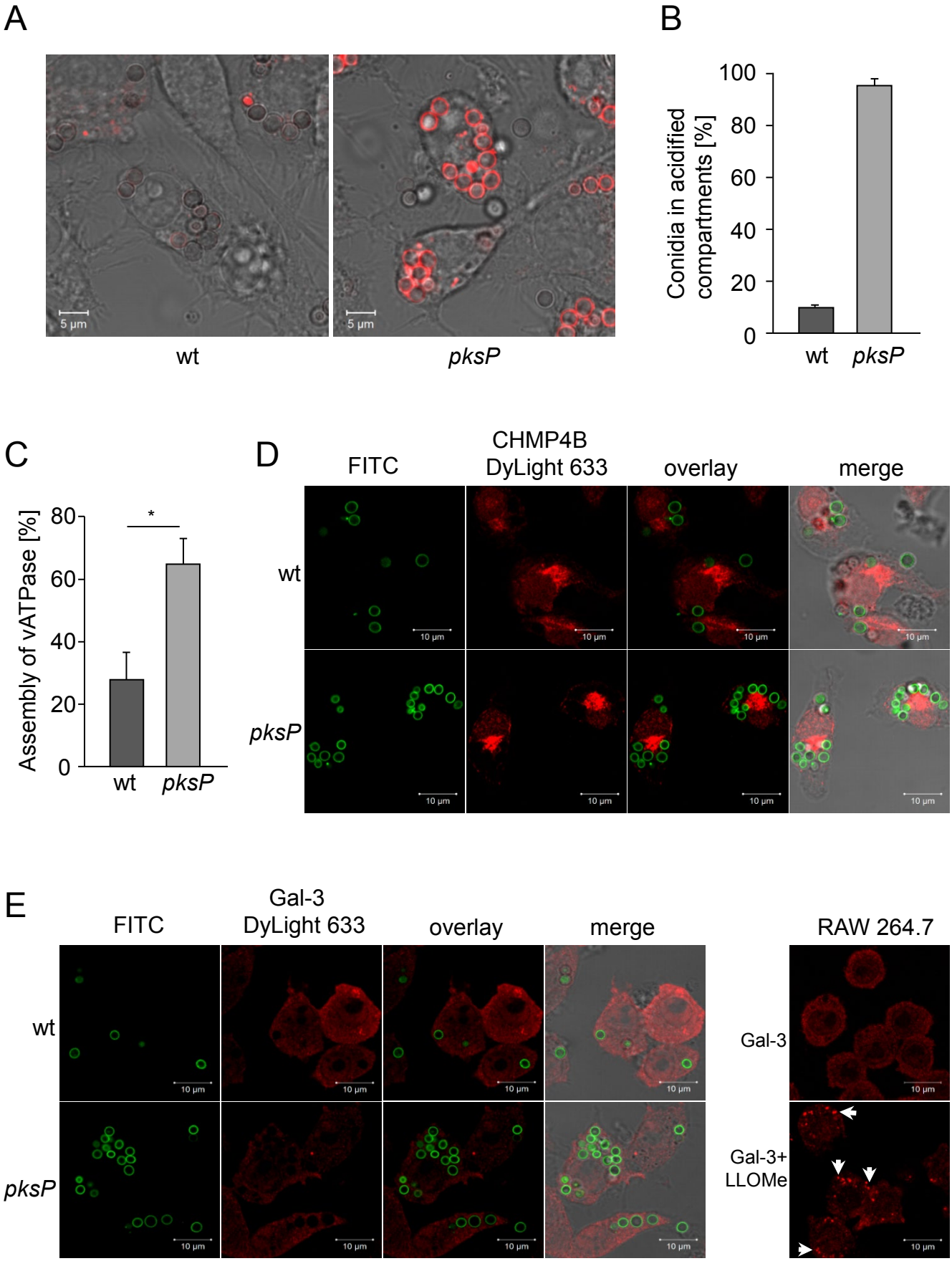
A
5 µm
5 µm
wt
pksP
B
Conidia in acidified compartments [%]
100
80
60
40
20
0
wt
pksP
C
Assembly of vATPase [%]
80
60
40
20
0
*
wt
pksP
D
FITC
CHMP4B DyLight 633
overlay
merge
wt
pksP
10 µm
E
FITC
Gal-3 DyLight 633
overlay
merge
wt
pksP
10 µm
RAW 264.7
Gal-3
Gal-3+ LLOMe
10 µm

Figure S1

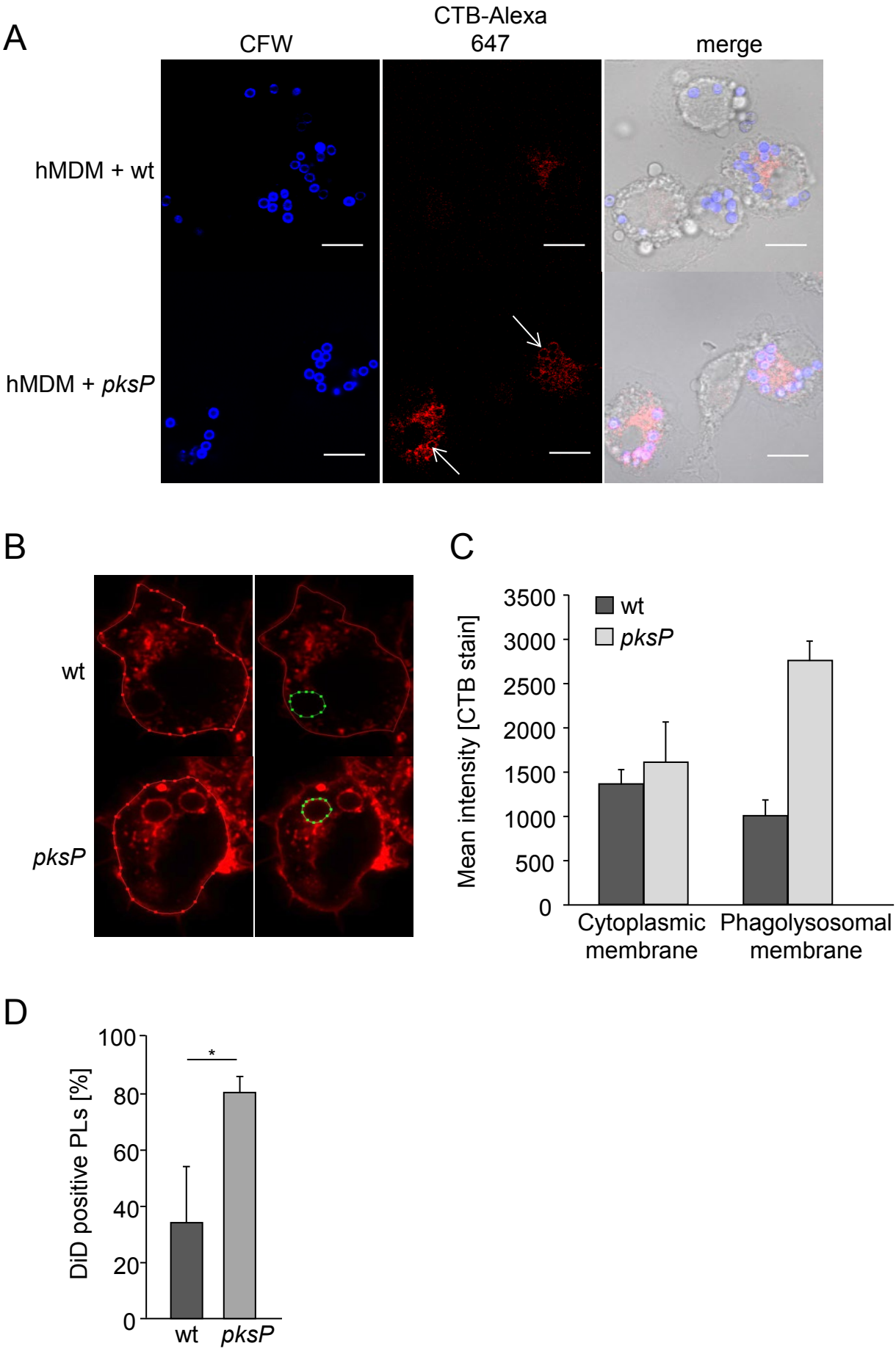
A
CFW
CTB-Alexa 647
merge
hMDM + wt
hMDM + pksP
B
wt
pksP
C
Mean intensity [CTB stain]
3500
3000
2500
2000
1500
1000
500
0
wt
pksP
Cytoplasmic membrane
Phagolysosomal membrane
D
DiD positive PLs [%]
100
80
60
40
20
0
*
wt
pksP

Figure S2

A

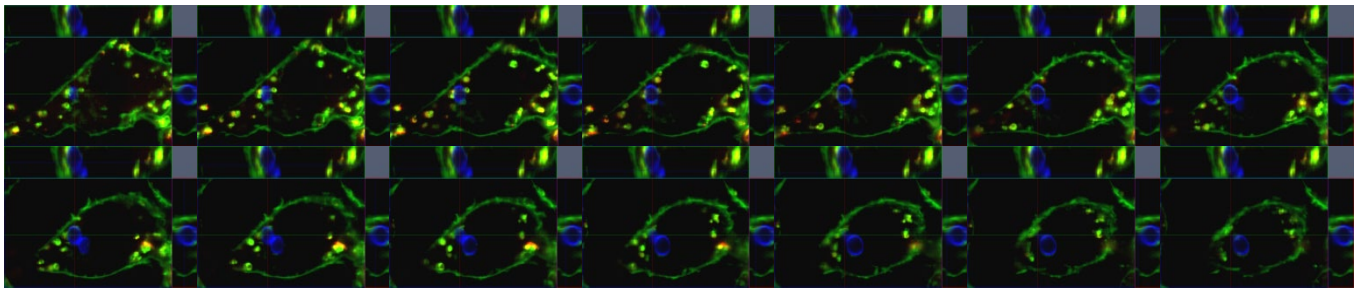

B

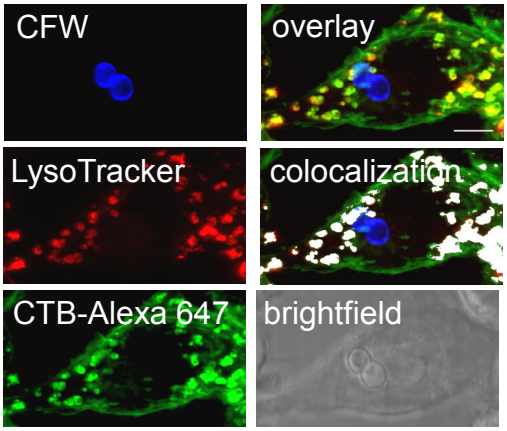

C

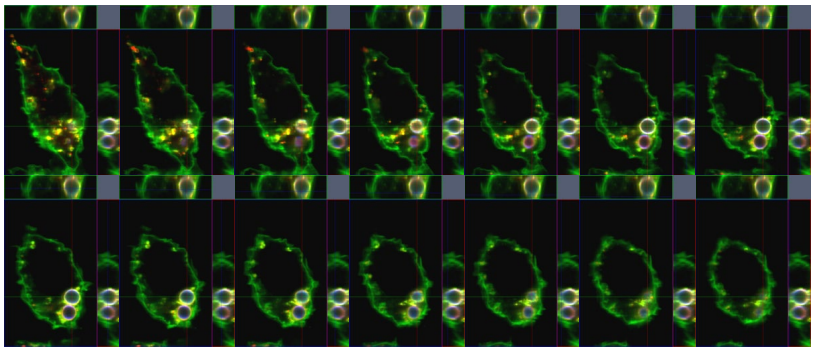

D

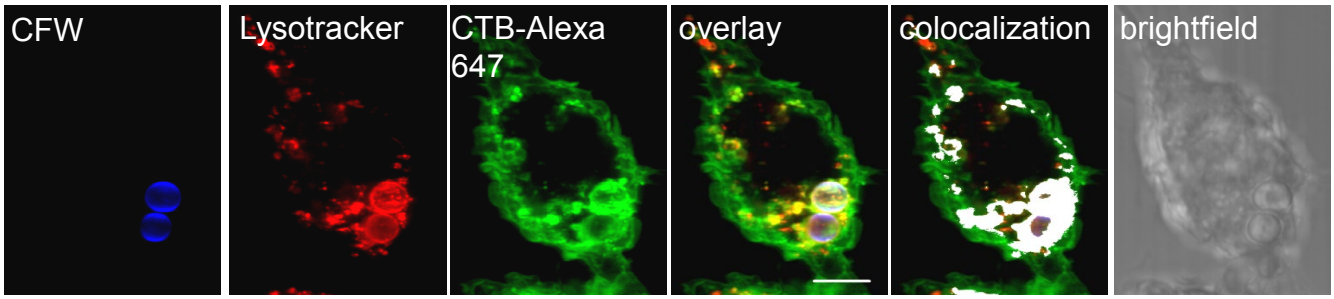

E

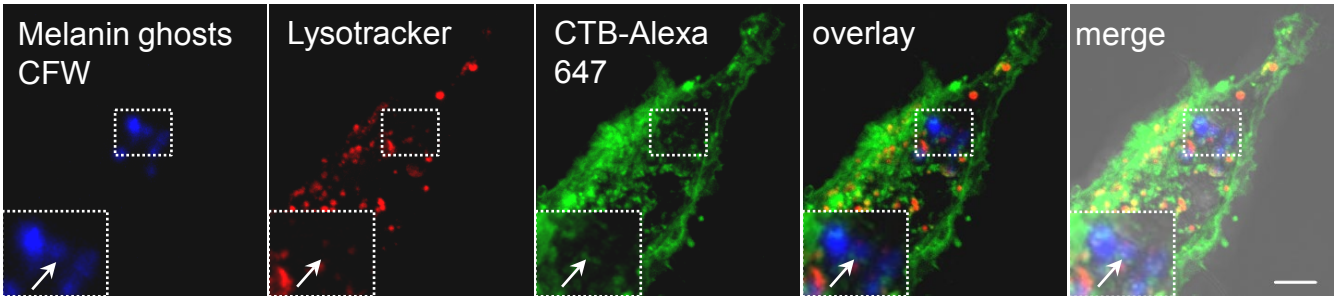

Figure S3

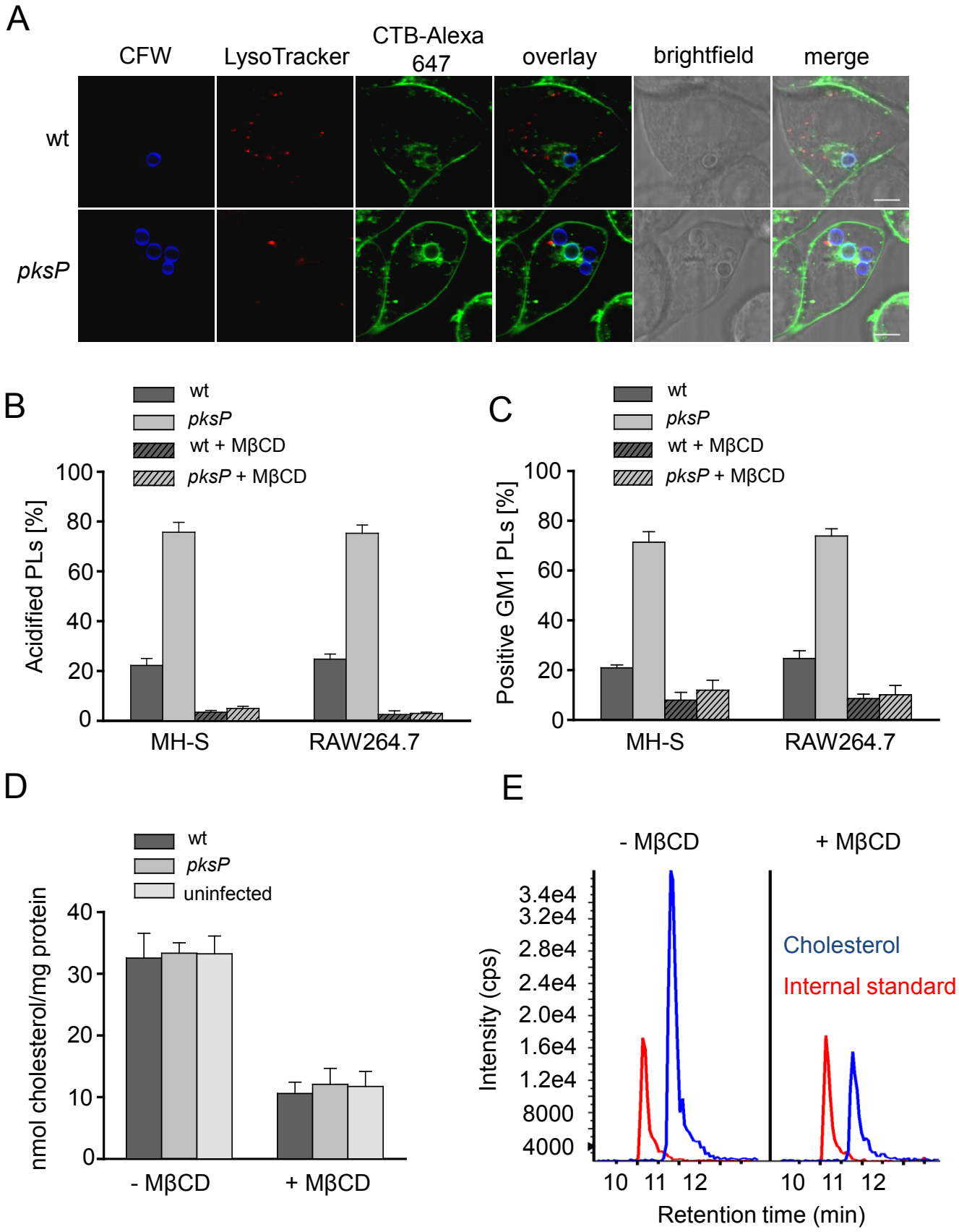
A
CFW
LysoTracker
CTB-Alexa 647
overlay
brightfield
merge
wt
pksP
B
wt
pksP
wt + MβCD
pksP + MβCD
Acidified PLs [%]
100
80
60
40
20
0
MH-S
RAW264.7
C
wt
pksP
wt + MβCD
pksP + MβCD
Positive GM1 PLs [%]
100
80
60
40
20
0
MH-S
RAW264.7
D
wt
pksP
uninfected
nmol cholesterol/mg protein
40
30
20
10
0
- MβCD
+ MβCD
E
- MβCD
+ MβCD
Intensity (cps)
3.4e4
3.2e4
2.8e4
2.4e4
2.0e4
1.6e4
1.2e4
8000
4000
Cholesterol
Internal standard
10
11
12
10
11
12
Retention time (min)

Figure S4

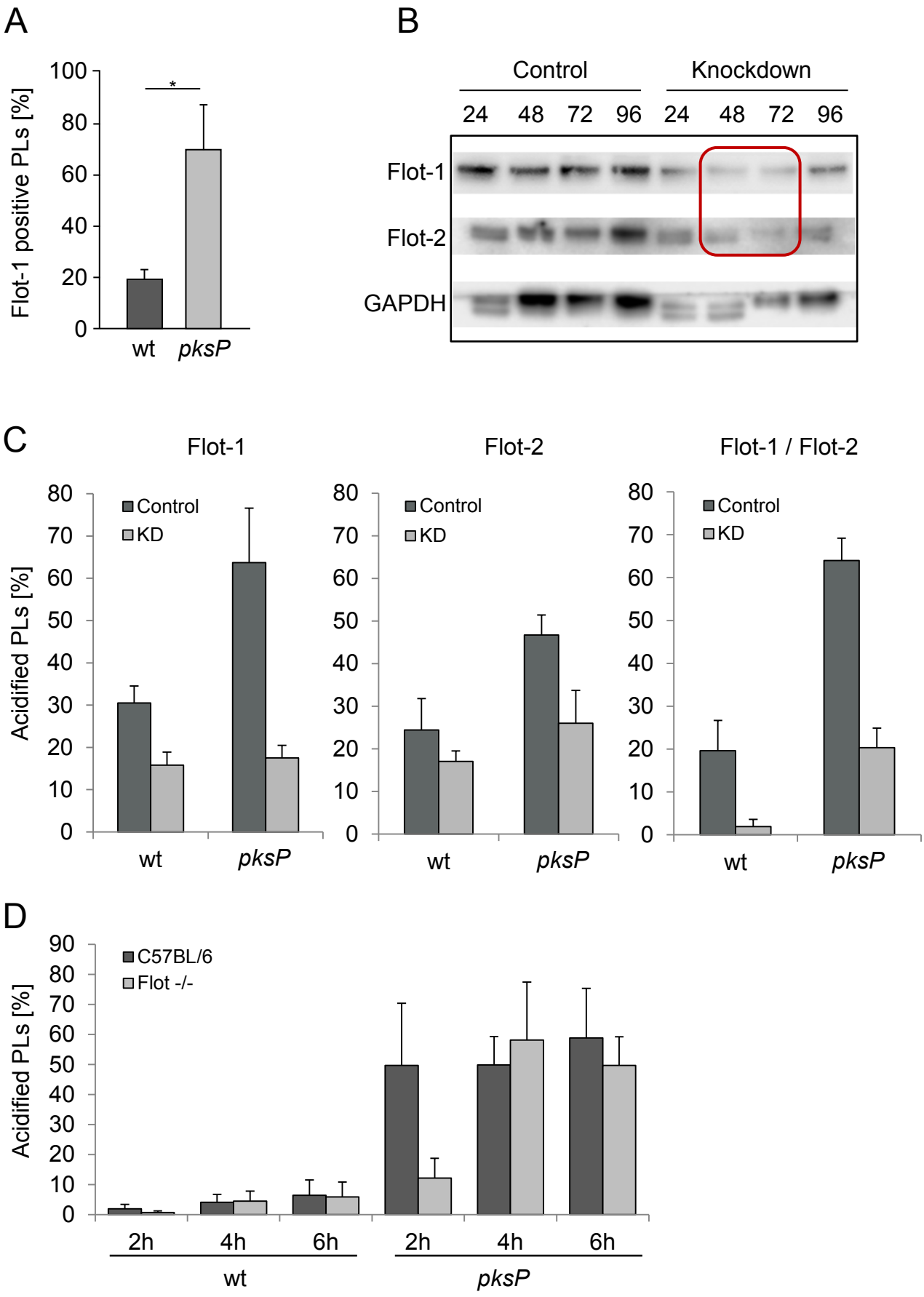
A
Flot-1 positive PLs [%]
100
80
60
40
20
0
*
wt
pksP
B
Control
Knockdown
24
48
72
96
24
48
72
96
Flot-1
Flot-2
GAPDH
C
Flot-1
Flot-2
Flot-1 / Flot-2
Acidified PLs [%]
Control
KD
wt
pksP
D
Acidified PLs [%]
C57BL/6
Flot -/-
2h
4h
6h
2h
4h
6h
wt
pksP

Figure S5

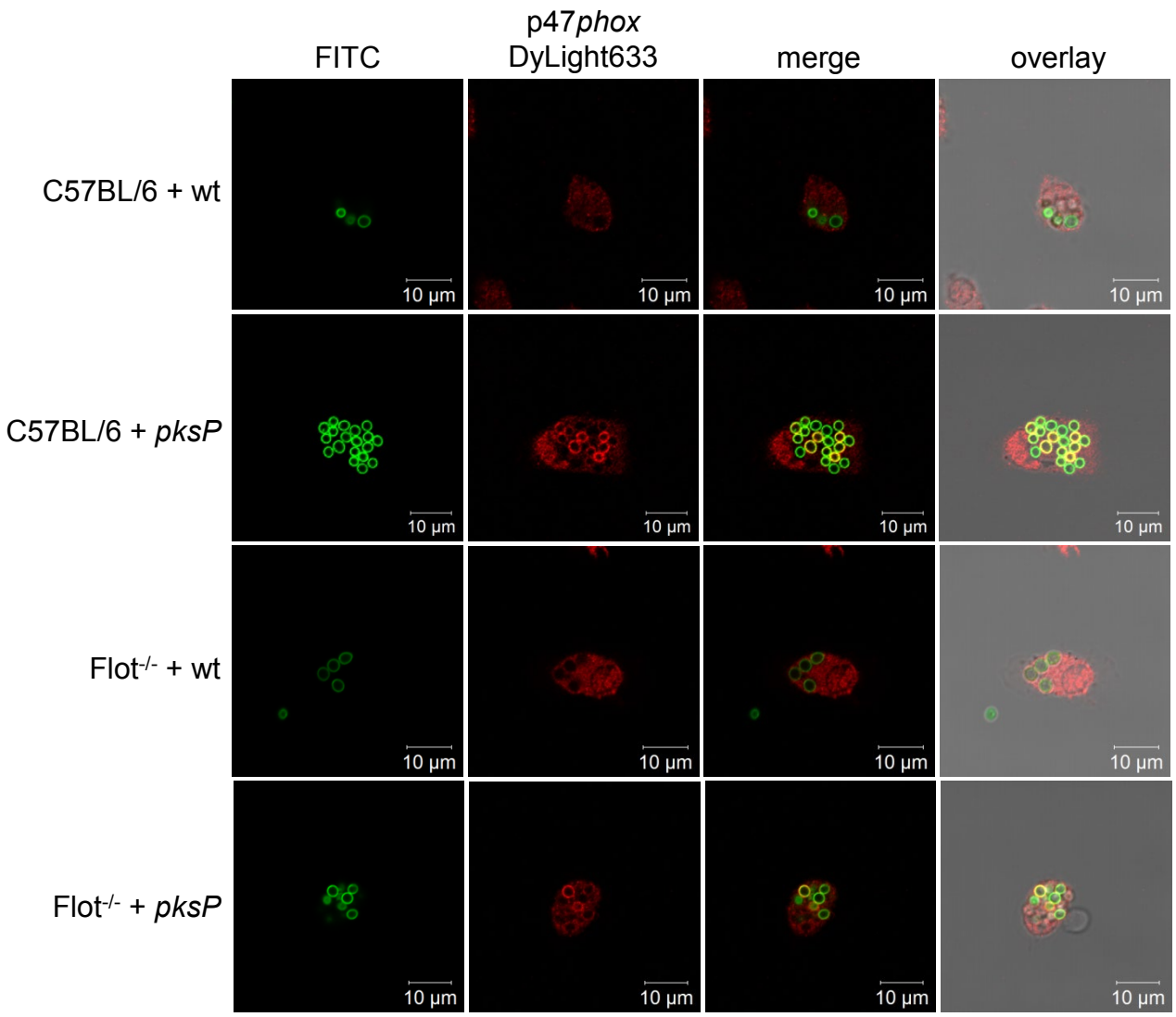
FITC
p47*phox*
DyLight633
merge
overlay
C57BL/6 + wt
C57BL/6 + *pksP*
Flot$^{-/-}$ + wt
Flot$^{-/-}$ + *pksP*
10 µm

Figure S6

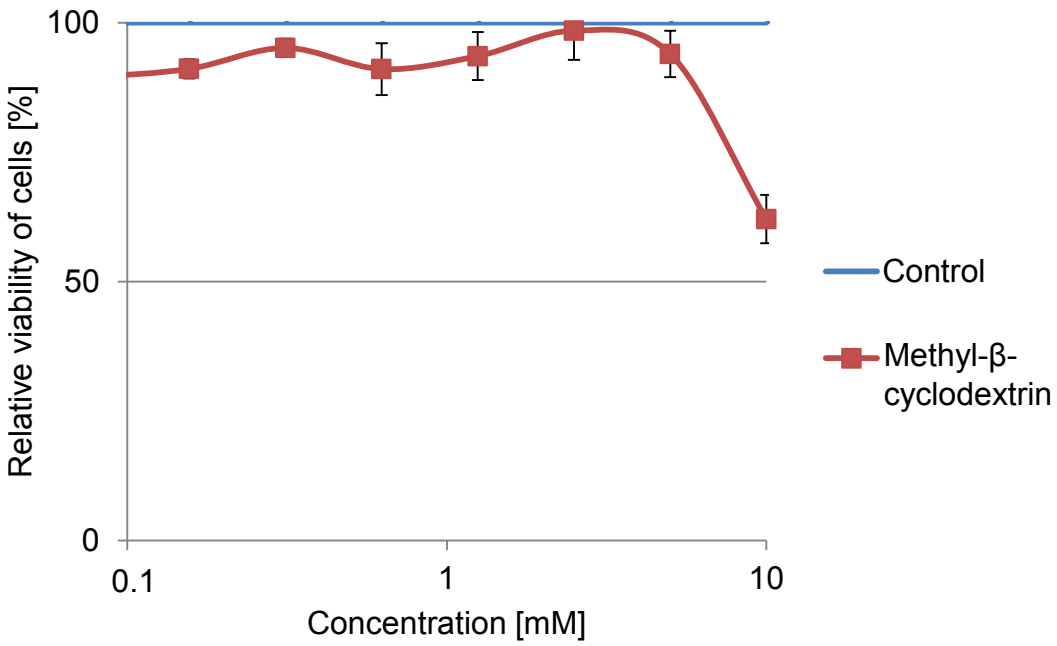
100
50
0
Relative viability of cells [%]
0.1
1
10
Concentration [mM]
Control
Methyl-β-cyclodextrin

Figure S7

SUPPLEMENTAL FIGURE TITLES AND LEGENDS

Figure S1 (related to Figure 1). **A)** Acidification of cellular compartments was measured with pHRodo. Conidia of the wild-type or *pksP* strain were labeled with pHRodo. RAW 264.7 cells were infected with conidia for 2 h at MOI = 2. Scale bar = 5 µm. **B)** Quantification of acidified cellular compartments in RAW 264.7 cells containing either wild-type or *pksP* conidia; at least 100 conidia were evaluated for the presence of a pHRodo signal. **C)** Melanin interferes with vATPase assembly at the phagolysosomal membrane. Assembly of vATPase (in percent) at the phagolysosomal membrane of RAW264.7 macrophages infected with wild-type and *pksP* conidia was quantified by immunofluorescence. Data represent mean values ± SD of at least 100 events per sample of three biological replicates in total; $p < 0.005$. **D)** and **E)** Phagolysosomes containing conidia are intact and not damaged after 2 hours of incubation. Immunofluorescence analysis of ESCRT III protein CHMP4B and galectin after 2 h of coincubation of RAW 264.7 macrophages with FITC-labeled wild-type and *pksP* conidia at MOI = 5. As positive control, LLOMe (Leu-Leu methyl ester hydrobromide) was used to damage phagosomes. Accumulation of galectin is indicated by white arrows. Scale bar = 10 µm.

Figure S2 (related to Figure 2). **A)** *A. fumigatus* conidia interfere with phagolysosomal GM1 ganglioside. Human monocyte-derived macrophages (hMDMs) were stained for GM1 ganglioside (CTB-Alexa 647, red) and were infected with CFW-labeled (blue) wild-type or *pksP* conidia. Scale bar = 10 µm. **B)** Reduction of GM1 in macrophages with phagocytosed wild-type conidia is restricted to the phagolysosomal membrane and not detected in the plasma membrane. RAW264.7 macrophages were stained for lipid rafts with CTB-Alexa 647 and infected with wild-type or *pksP* conidia. **C)** The cytoplasmic and phagolysosomal GM1 signals were quantified by measuring the mean intensity of the marked areas using the Zen 2.3 software. **D)** Melanin interferes with lipid composition at the phagolysosomal membrane. Ratio (in percent) of DiD-positive phagolysosomes (PLs). RAW264.7 macrophages were treated with

DiD and cells were infected with *pksP* and wild-type conidia. At least 100 events per sample of three biological replicates in total were quantified. Columns represent mean values ± SD; $p < 0.05$.

Figure S3 (related to Figure 2). **A-D)** Lysosomal vesicles co-localize with membrane microdomains. Z-scan of CFW-labeled wild-type (blue) (A, B) and *pksP* conidia (blue) (C, D) after 2 h of phagocytosis by RAW264.7 macrophages stained with LysoTracker Red (red) and CTB-Alexa Fluor 647 (green). Orthoview of Z-stack with increments of 0.34 μm in overlay mode (A, C) and corresponding maximum intensity projection (B, D) of the single channels: CFW-labeled conidia (blue), LysoTracker (red), CTB-Alexa Fluor 647 (green), overlay, co-localization of LysoTracker Red and CTB-Alexa Fluor 647 in overlay mode (white), brightfield merged with overlay image. Scale bar = 5 μm. **E)** DHN-melanin prevents formation of membrane microdomains and acidification of phagolysosomes. DHN-melanin ghosts (labeled with CFW, blue) were incubated with RAW264.7 macrophages. Acidification of melanin ghosts-containing phagolysosomes was monitored by LysoTracker Red staining and recruitment of GM1 was visualized by CTB-Alexa Fluor 647 staining. Melanin ghosts had the same capacity as wild-type conidia to prevent phagolysosomal acidification and block the formation of microdomains in the phagolysosomal membrane (white arrow).

Figure S4 (related to Figure 2). Cholesterol depletion inhibits phagolysosomal acidification. **A)** Impact of MβCD-treatment on acidification of membrane microdomains-containing phagolysosomes after 2 h of phagocytosis of CFW-labeled wild-type or *pksP* conidia (blue) by RAW264.7 macrophages stained with LysoTracker (red) and CTB-Alexa Fluor 647 (green). Data represent mean values of at least 100 events per replicate of three biological replicates in total ± SD; Scale bar = 5 μm. **B)** and **C)** Microscopic determination in two different macrophage cell lines; (B) percentage of conidia-containing acidified phagolysosomes; (C) localization of membrane microdomains of the respective samples in the presence or absence of MβCD. Data

represent mean values ± SD of three experiments. **D)** Quantification of cellular cholesterol in the presence or absence of MβCD. Data represent mean values ± SD. **E)** Representative LC-MS-chromatogram of cholesterol quantification.

Figure S5 (related to Figure 4). Flotillins are required for acidification of conidia-containing phagolysosomes (PLs). **A)** Different amounts of Flot-1 in conidia-containing phagolysosomes. RAW264.7 macrophages were incubated with wild-type and *pksP* conidia. Phagolysosomes were isolated and Flot-1 was detected by immunofluorescence using an anti-Flotillin-1 antibody. We quantified at least 100 events per sample of three biological replicates. Data are presented as mean ± SD. $p < 0.05$. **B)** Western blot using Flot-1 and Flot-2 antibodies to monitor reduced flotillin protein levels in J774A.1 macrophages after transfection with Flot-1 and Flot-2 siRNA and incubation for 24, 48, 72 and 96 h with *A. fumigatus* wild-type conidia. **C)** Quantification of acidified conidia-containing phagolysosomes (PLs) after knockdown (KD) of Flot-1, Flot-2 or double knockdown of Flot-1 and Flot-2. Data represent mean values ± SD. **D)** Time course of acidification of conidia-containing phagolysosomes of wild-type or $Flot^{-/-}$ BMDMs. Data are presented as mean ± SD. We quantified at least 100 events per sample of three biological replicates in total.

Figure S6 (related to Figure 5). DHN-melanin reduces NADPH oxidase assembly on the phagolysosomal membrane. BMDMs were isolated from wild-type (C57BL/6) and $Flot^{-/-}$ mice. Assembly of the NADPH oxidase complex on conidia-containing phagolysosomal membranes was monitored by immunolabeling of p47*phox* (red). Conidia were stained with FITC (green).

Figure S7 (related to STAR Methods). Cytotoxicity of MβCD on RAW264.7 macrophages after incubation for 4 h. Viability was measured by Resazurin assay and relative viability is given for treated cells against untreated cells (control).